Recent Science with Synchrotron Radiation

Sunil K. Sinha

UCSD

Cheiron School 2011 Lecture

Science with X-Rays

- Diffraction and crystal structures
- Structure Factors of liquids and glasses
- Structures of Thin Films
- ARPES
- EXAFS, XANES
- Studies of Magnetism with resonant XMS
- Inelastic X-ray scattering: phonons, electronic excitations
- X-ray Photon Correlation Spectroscopy
- Microscopy
- Imaging/Tomography
- Pump-Probe Studies

Compare the evolution of high intensity optical and x-ray sources

Hign-intensity at optical wavelengths
- high harmonic generation
- tabletop coherent x-ray radiation
- attosecond pulses

High-intensity at x-ray wavelengths

?

?

?

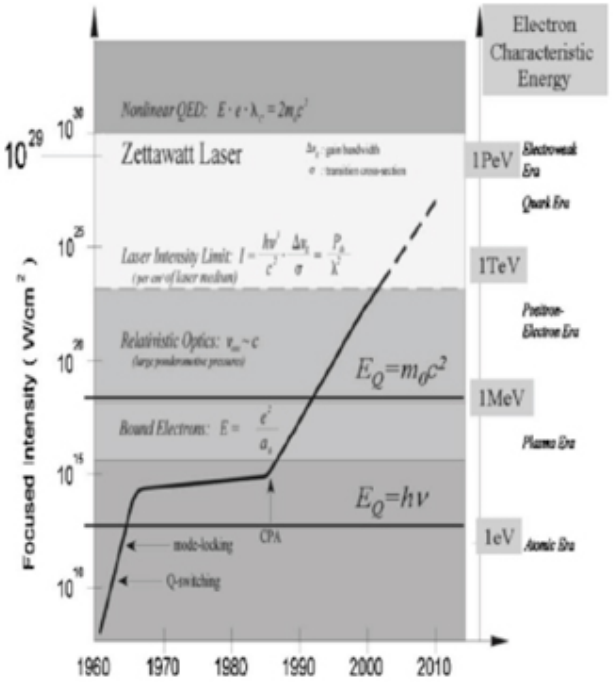

G. Mourou RMP 2006

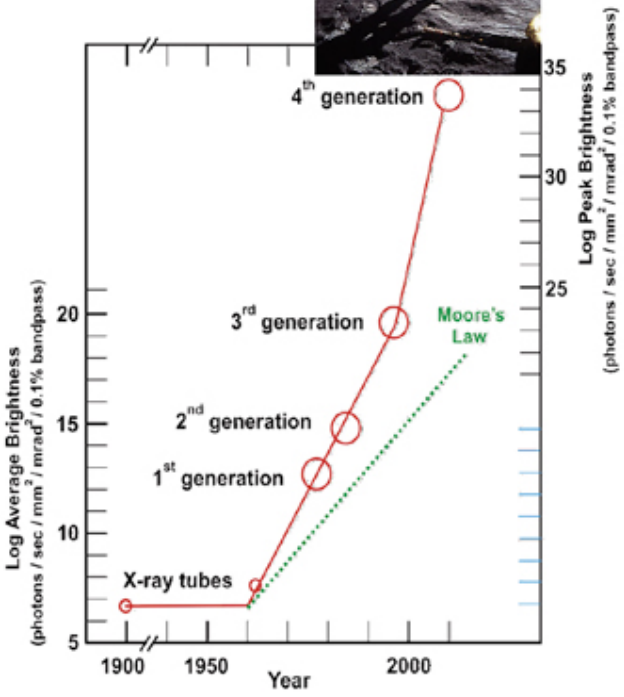

D. Moncton, George Brown

Example 1: X-Ray Diffraction & structural biology

- D.C. Phillips presents the 3-D structure of lysozyme to the Royal Society in **1965**
- Linear polypeptide chain
- Folded model of the same amino acid sequence
- July 2009: 58,588 structures in Protein Data Bank

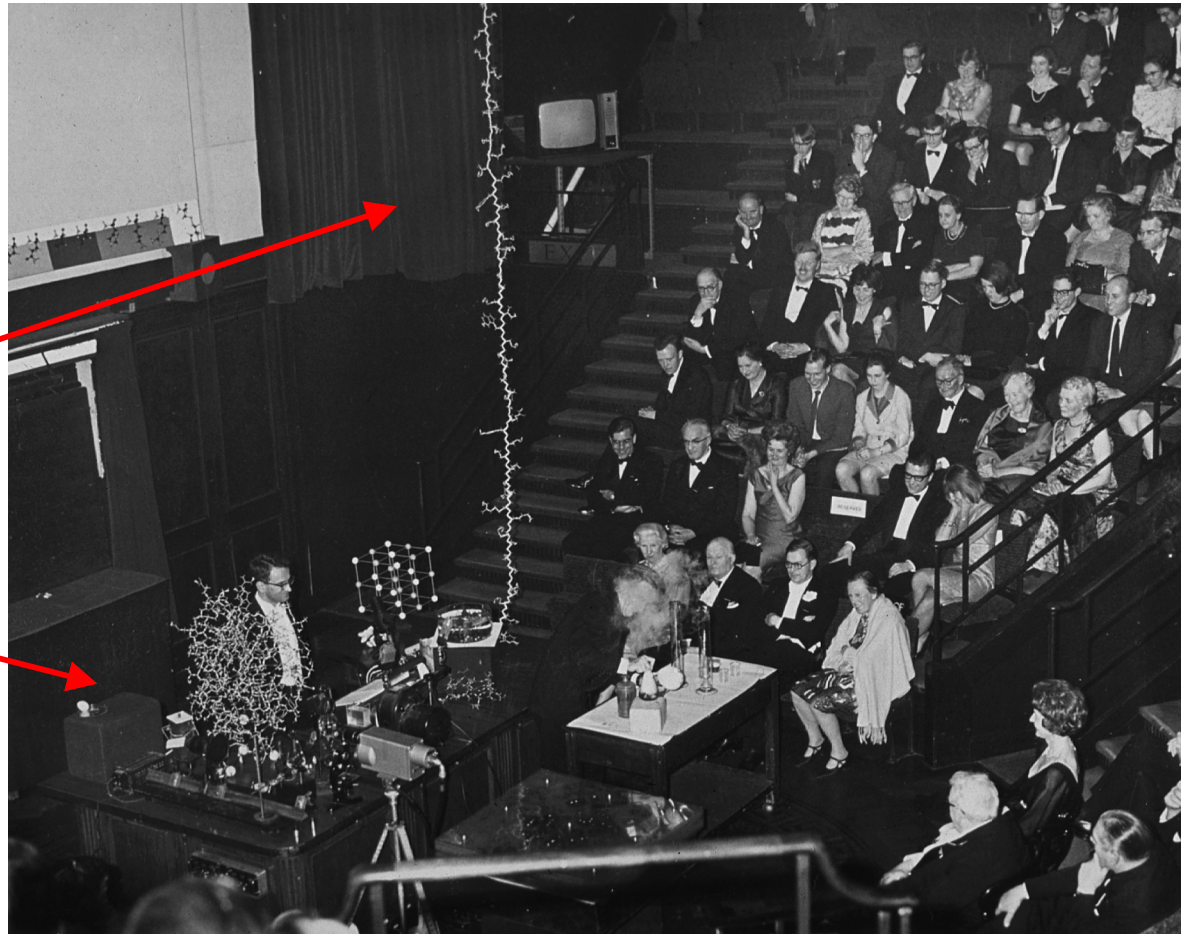

A single protein structure used to be the project of a scientific lifetime

Synchrotron Radiation - 8301 structures solved in 2009

Synchrotron research on proteins has led to major advances in drugs to battle infection, HIV, cancer

Renal cancer drug pazopanib™ developed in part based on APS research (GlaxoSmithKline)

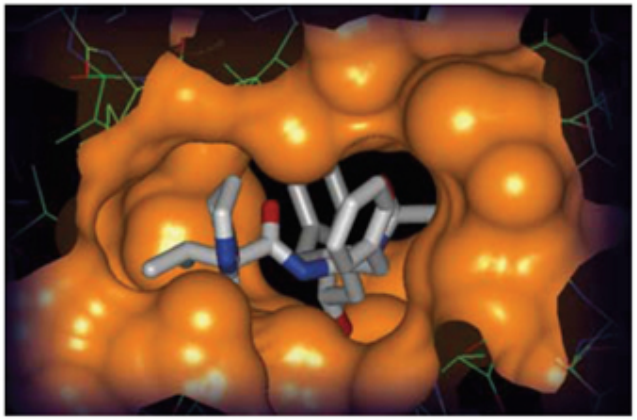

Close-up view of the drug binding site within HIV protease (Kaletra®, Abbott).

Ramakrishnan, Steitz and Yonath
2009 Chemistry Nobel Laureates

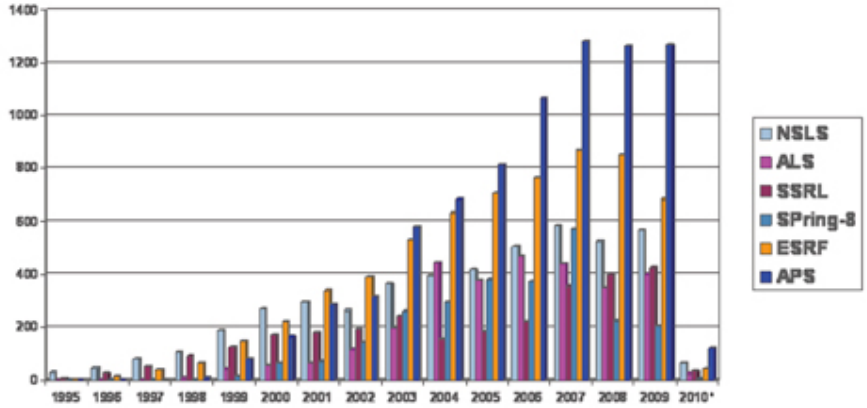

APS protein structure output is almost twice that of any other light source

X-rays dominant in protein structure determinations

WORLDWIDE PDB
PROTEIN DATA BANK

Snapshot: July 1, 2009

58,588 released atomic coordinate entries

Molecule Type

54,141	proteins, peptides, and viruses
2,033	nucleic acids
2,381	protein/nucleic acid complexes
33	other

Experimental Technique

50,284	X-ray
7,914	NMR
243	electron microscopy
17	hybrid
130	other

Year	Total Depositions
2000	2983
2001	3286
2002	3563
2003	4830
2004	5508
2005	6678
2006	7282
2007	8130
2008	7073
2009	8301
2010	1952
TOTAL	59586

Designing antibiotics -

difference between bacterial and eukaryotic ribosomes is one amine group in the 2.5MD ribosome

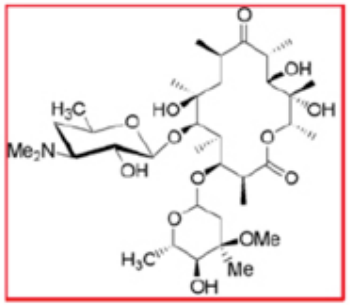

Erythromycin – a macrolide antibiotic that blocks protein synthesis by binding to bacterial ribosomes but not to eukaryotic ribosomes

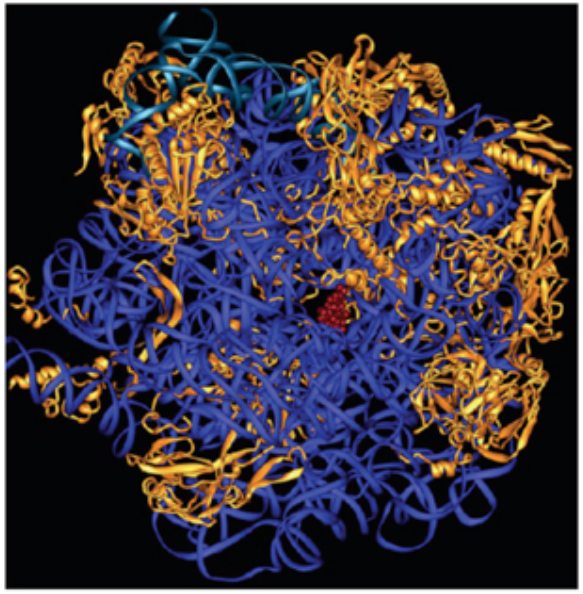

www.molgen.mpg.de

Basics of Resonant X-ray Magnetic Scattering

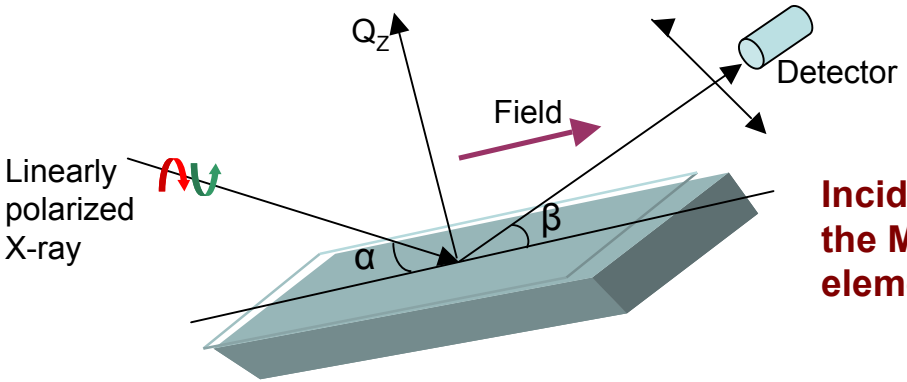

Incident x-rays are tuned to the M edges of rare earth element (in this case Dy)

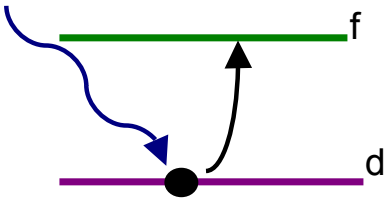

The scattering factor in the dipole approximation is given by,

$$f = (\boldsymbol{e}_s^*.\boldsymbol{e}_i)\left\{-r_e Z + \frac{3}{8\pi}\lambda[F_1^1 + F_{-1}^1]\right\} + \frac{3}{8\pi}\lambda i(\boldsymbol{e}_s^* \times \boldsymbol{e}_i)\cdot\boldsymbol{m}[F_{-1}^1 - F_1^1] + (\boldsymbol{e}_s^*.\boldsymbol{m})(\boldsymbol{e}_i.\boldsymbol{m})[2F_0^1 - F_1^1 - F_{-1}^1]$$

f_C - charge scattering factor

f_m - magnetic scattering factor

- $I_\sigma \propto |f_C|^2 + |f_m|^2$

- **Total signal is combination of charge and relatively weaker magnetic signal. For charge forbidden Bragg peak, signal is dominated by magnetic contributions.**
- **The signal in the case of Dy is due to antiferromagnetic Bragg peak.**

Depth Dependent Magnetic Density Profile

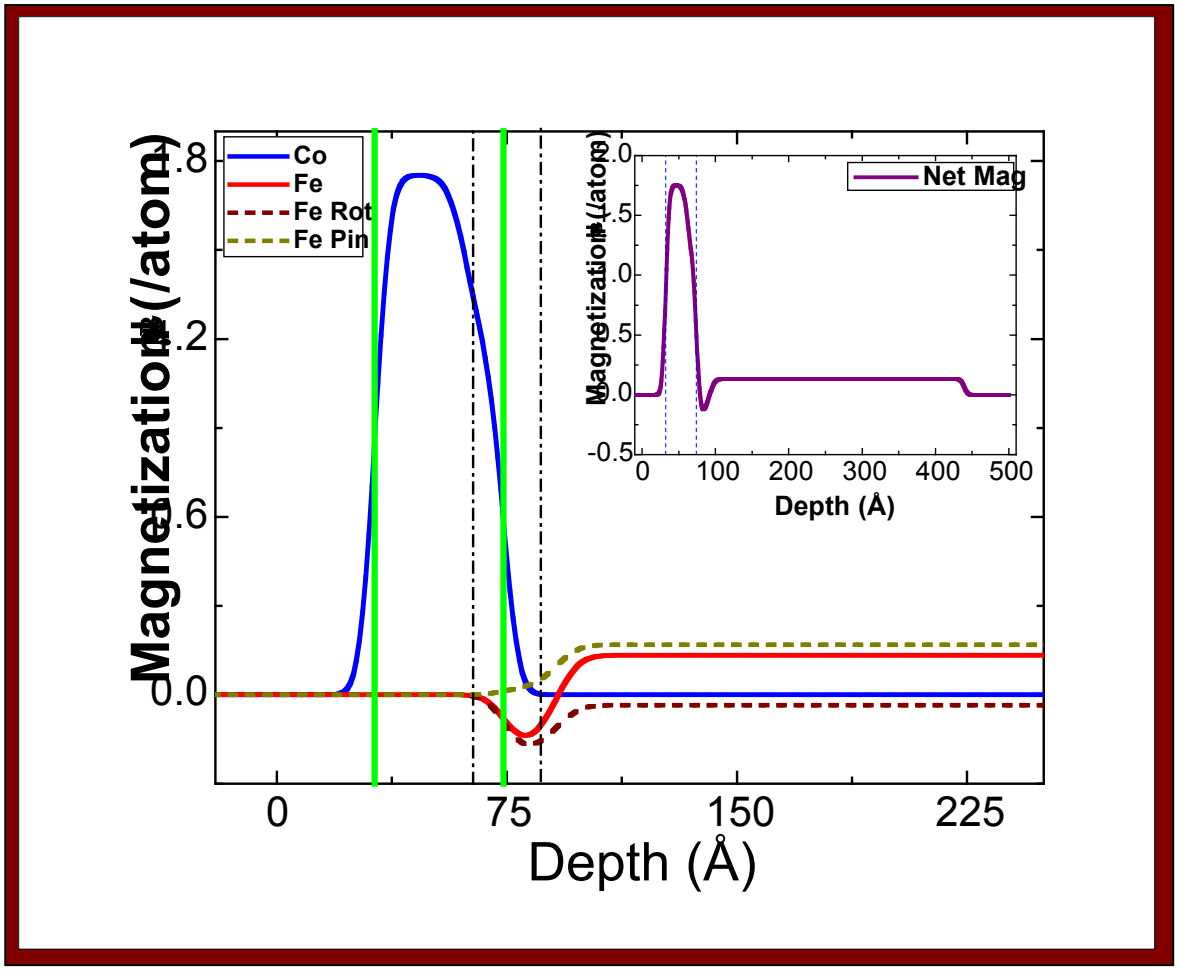

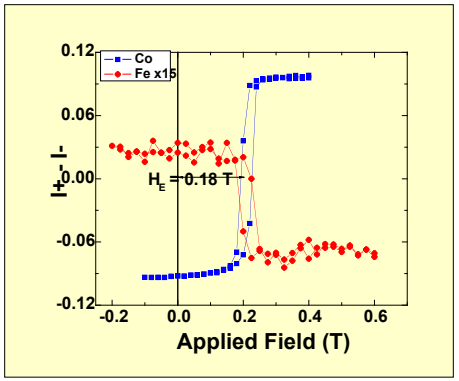

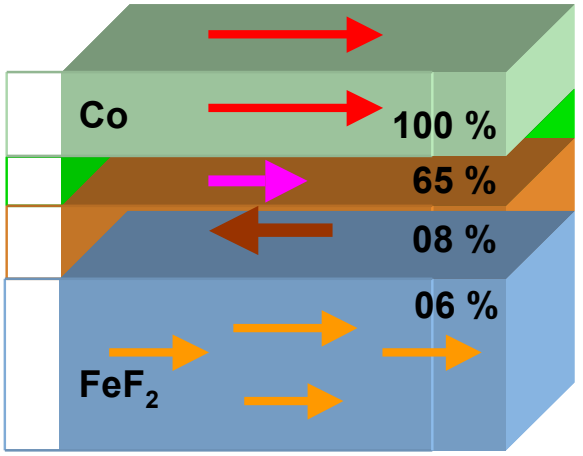

Exchange bias due to exchange interaction between Fe pinned and Co moment across the Co/FeF_2 interface.

Polarons via single-crystal diffuse scattering

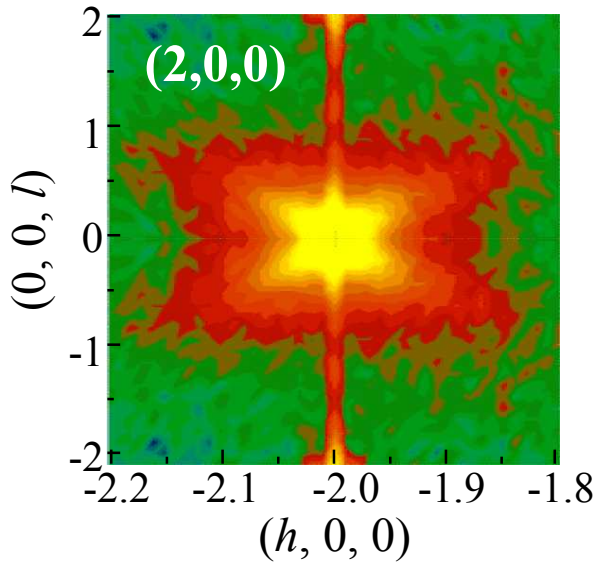

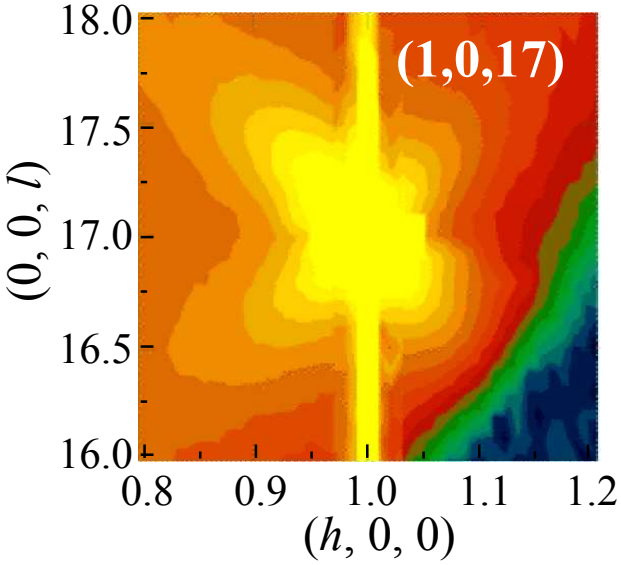

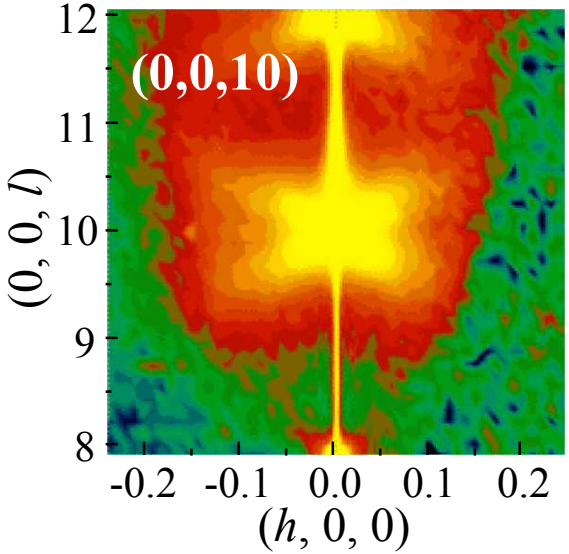

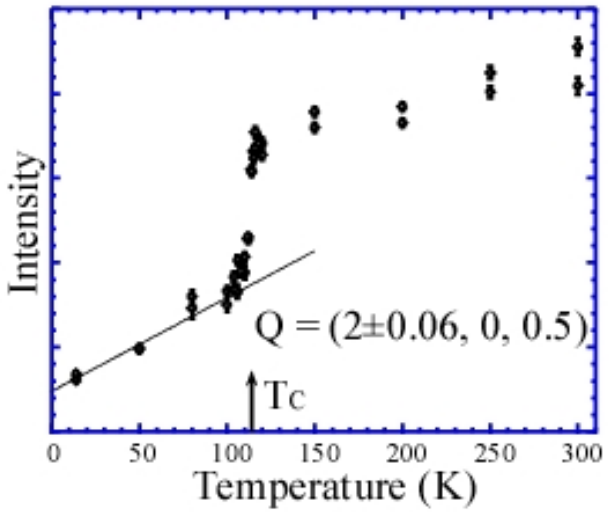

L. Vasiliu-Doloc *et al.*, PRL **83**, 4393 (1999).

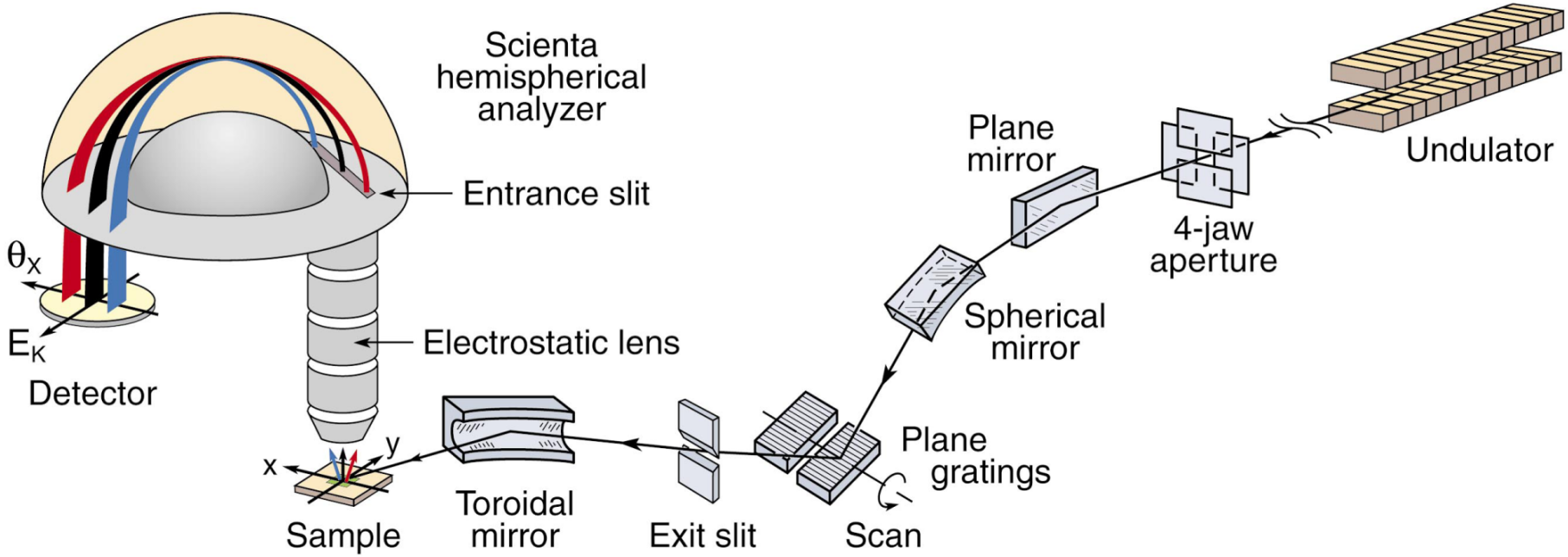

IG. 6. Generic beamline equipped with a plane grating monochromator and a Scienta electron spectrometer (Color).

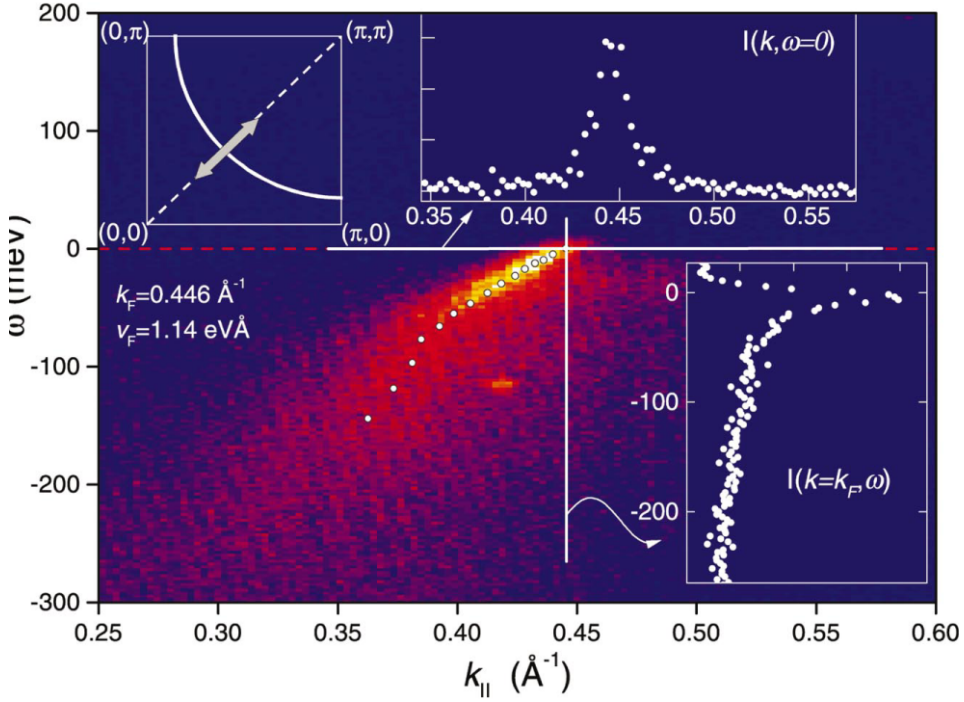

IG. 7. Energy (ω) vs momentum ($\mathbf{k}_{\|}$) image plot of the pho-
)emission intensity from $Bi_2Sr_2CaCu_2O_{8+\delta}$ along (0,0)-(π,π).
his k-space cut was taken across the Fermi surface (see
ketch of the 2D Brillouin zone upper left) and allows a direct
sualization of the photohole spectral function $A(\mathbf{k},\omega)$ (al-
nough weighted by Fermi distribution and matrix elements).
he quasiparticle dispersion can be clearly followed up to E_F,
s emphasized by the white circles. Energy scans at constant
nomentum (right) and momentum scans at constant energy
pper right) define *energy distribution curves* (EDC's) and
omentum distribution curves (MDC's), respectively. After
alla, Fedorov, Johnson, Wells, *et al.*, 1999 (Color).

TOPOLOGICAL INSULATORS AND DIRAC POINTS

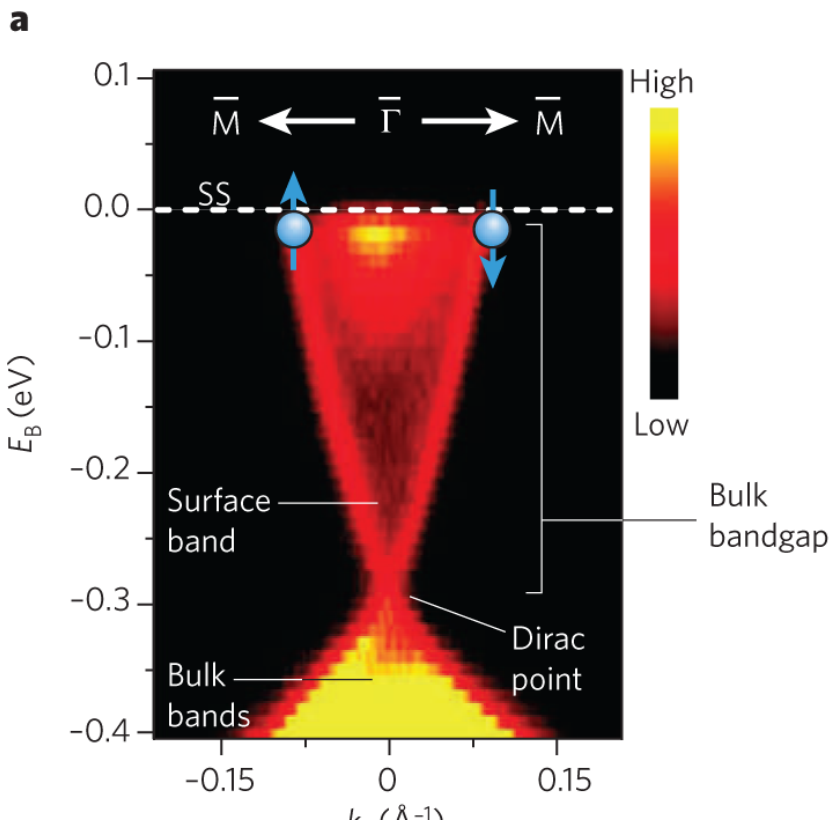

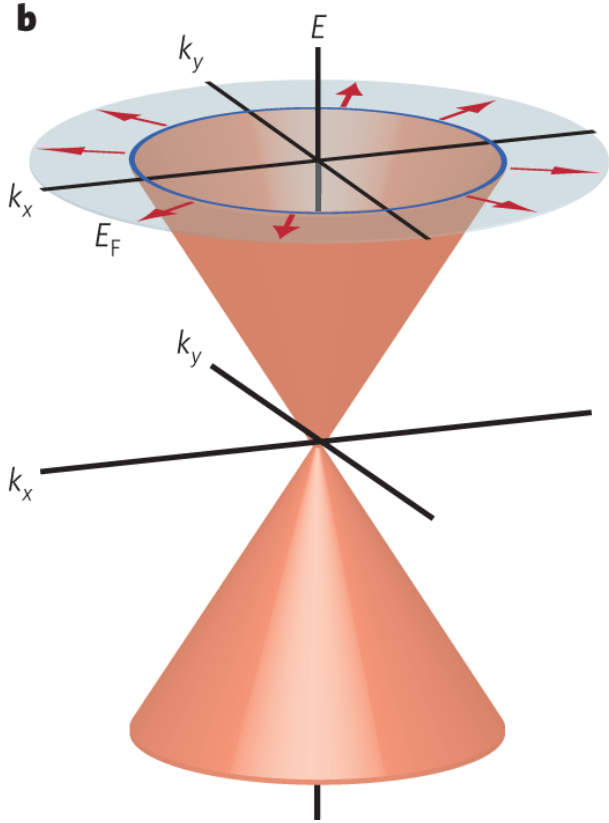

Phase Contrast Imaging
PEEM
X-ray tomography
X-ray Microscopy/Fluorescence microscopy
X-Ray Holography
Phase retrieval imaging

Phase enhanced x-ray imaging:

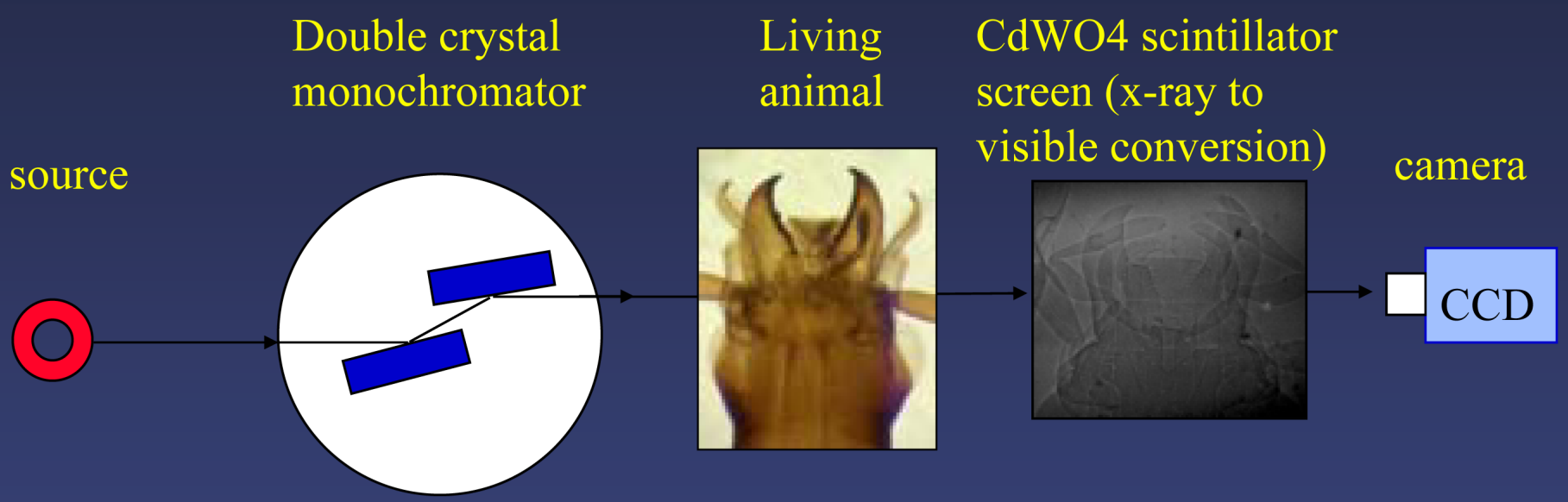

X-ray images depend on differences in density within the sample.

Also: Beam coherence produces interference fringes (edge enhancement effects).

COHERENT X-RAY BEAMS

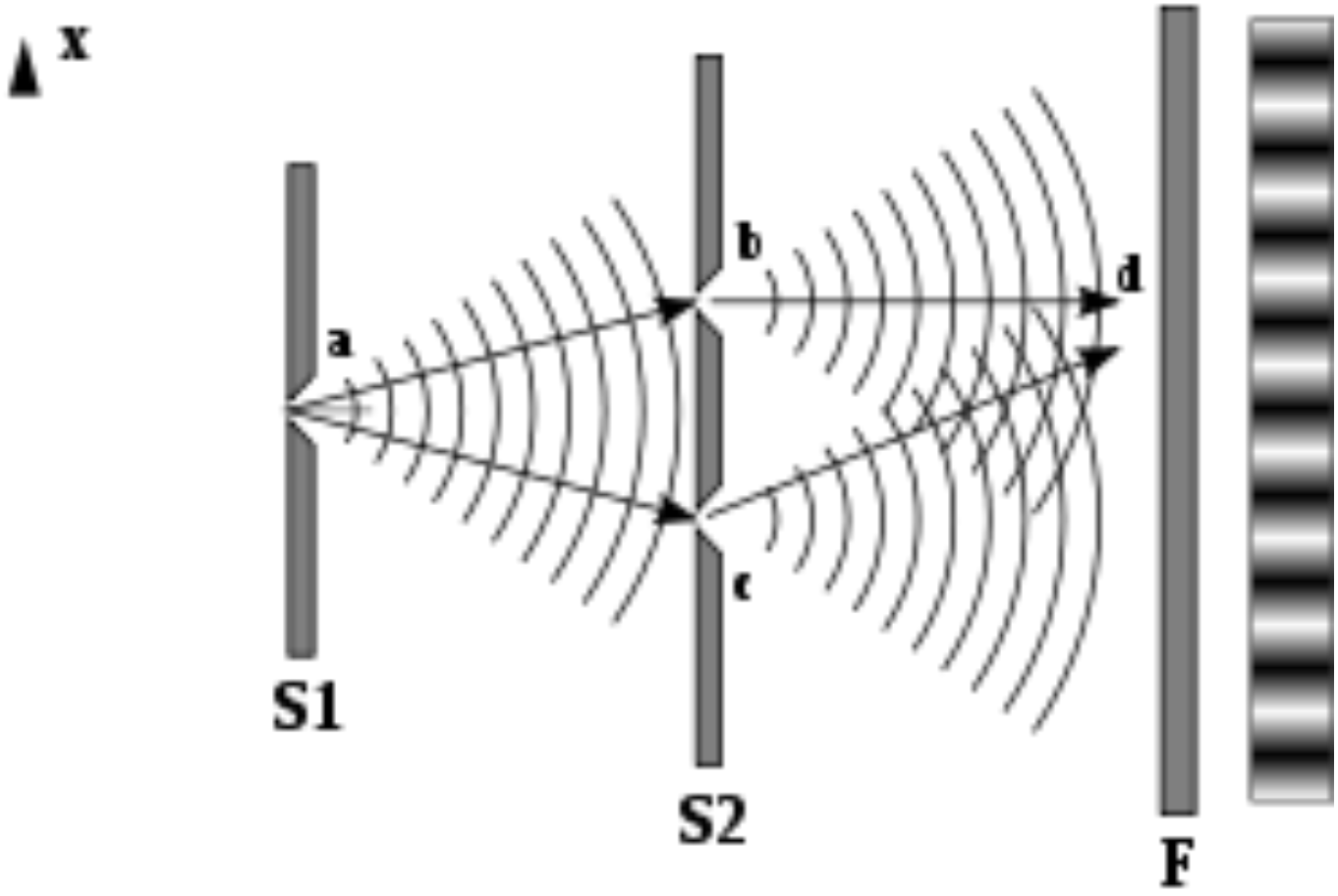

Coherence Lengths

$\xi_l = \lambda^2 / \Delta\lambda$
$= \lambda(\Delta\lambda/\lambda)^{-1}$

$\xi_t = \lambda R / s$
$(\xi_{hor.}, \xi_{vert.})$

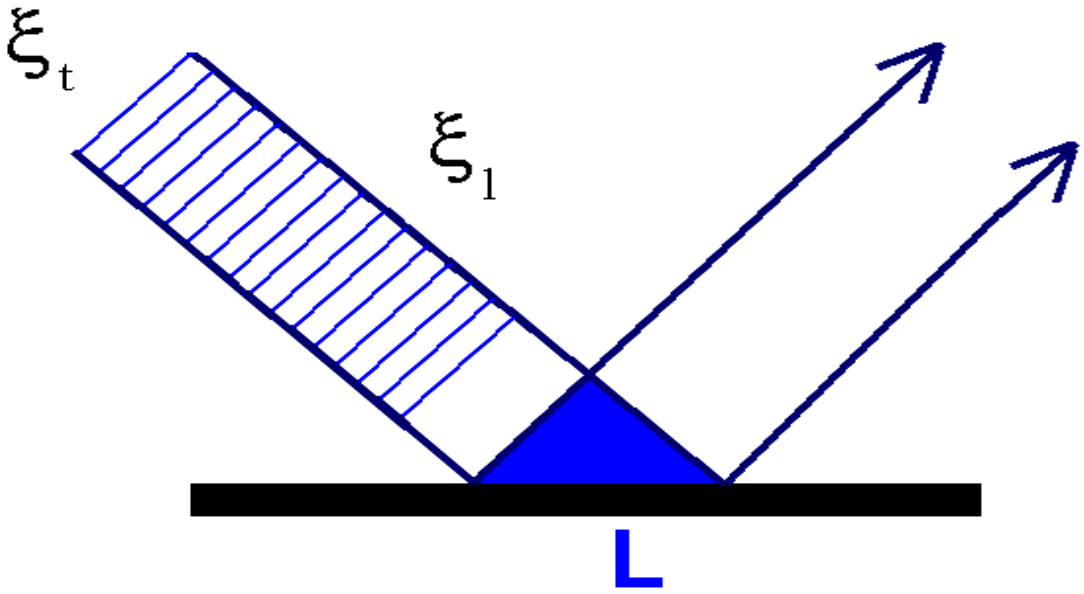

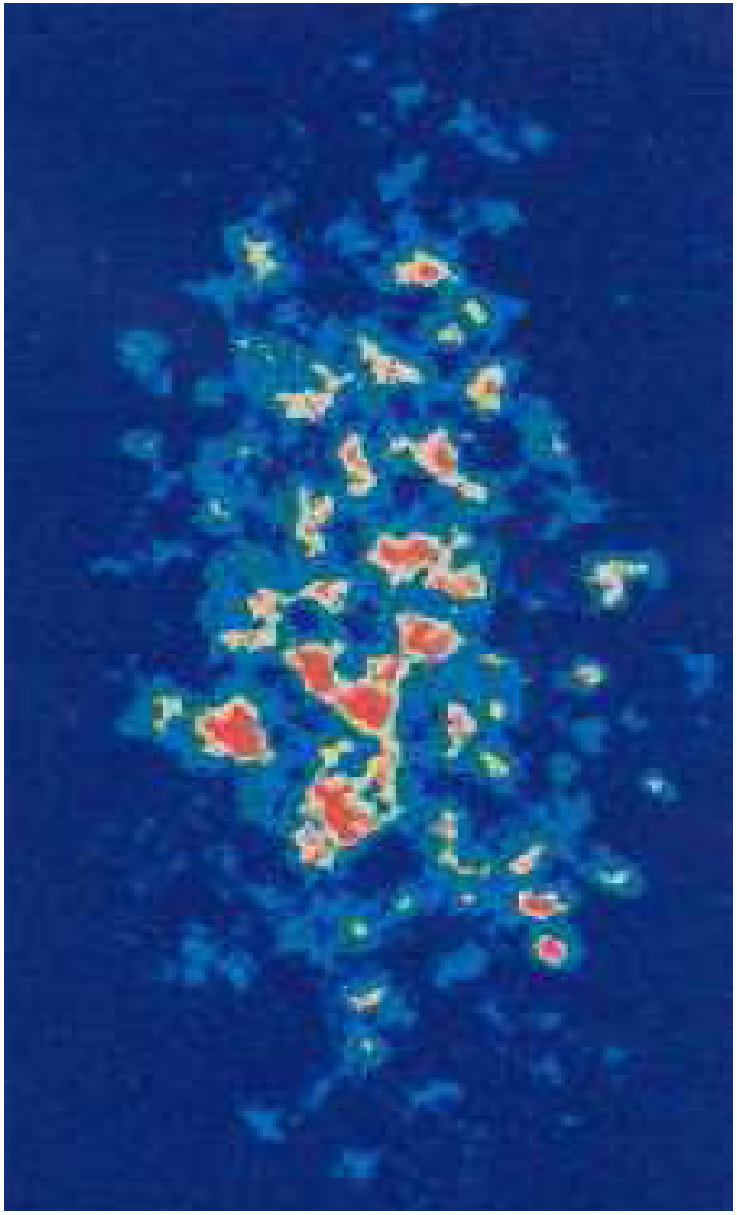

First X-ray Speckle:
M. Sutton et al., *Nature* **352**, 608-610 (1991)

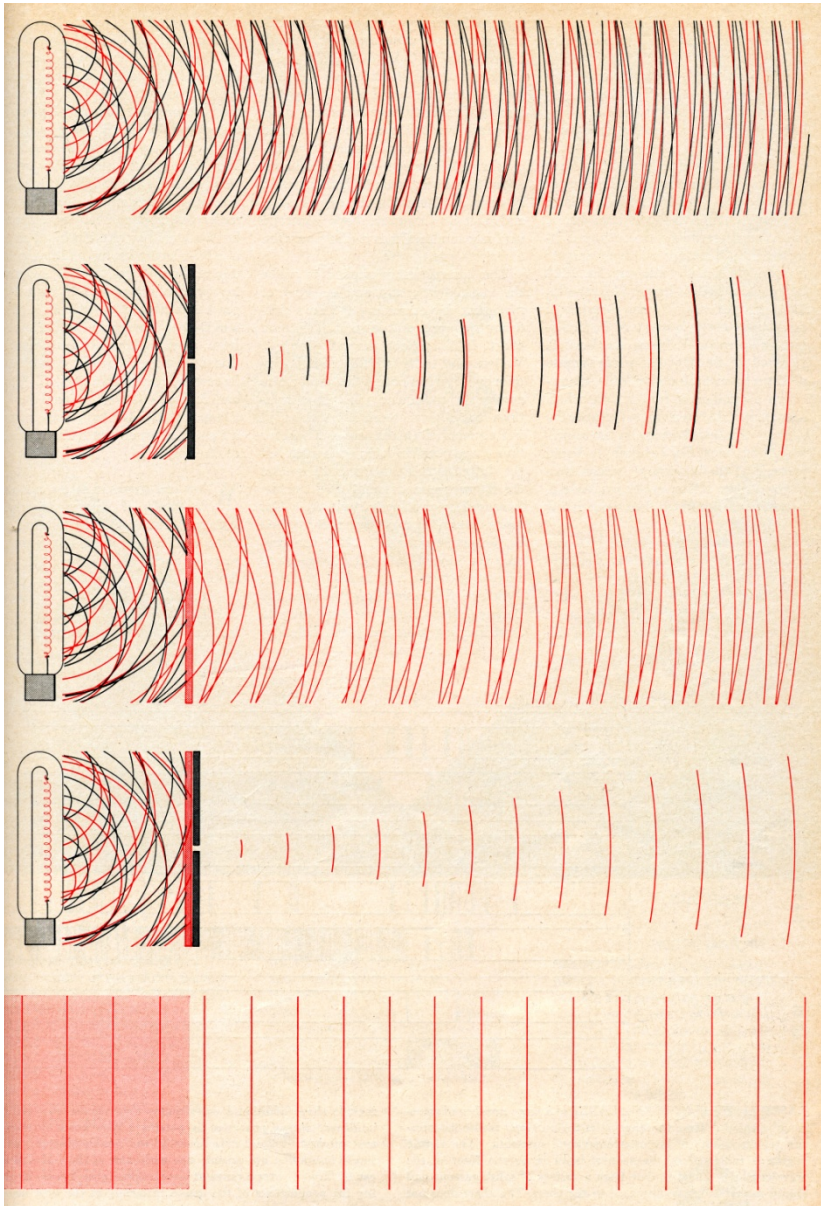

A. L. Schawlow "Laser Light"
Scientific American, 219 (3), p. 120, (1968)

Imaging via Soft X-ray Fourier Transform Holography

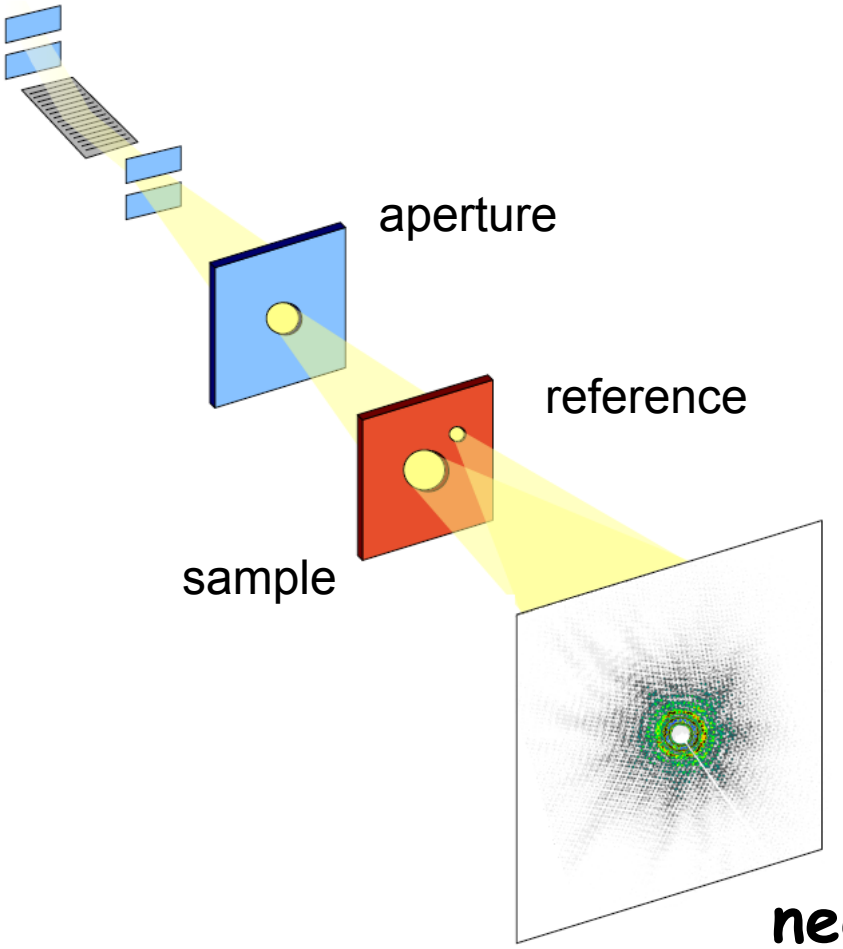

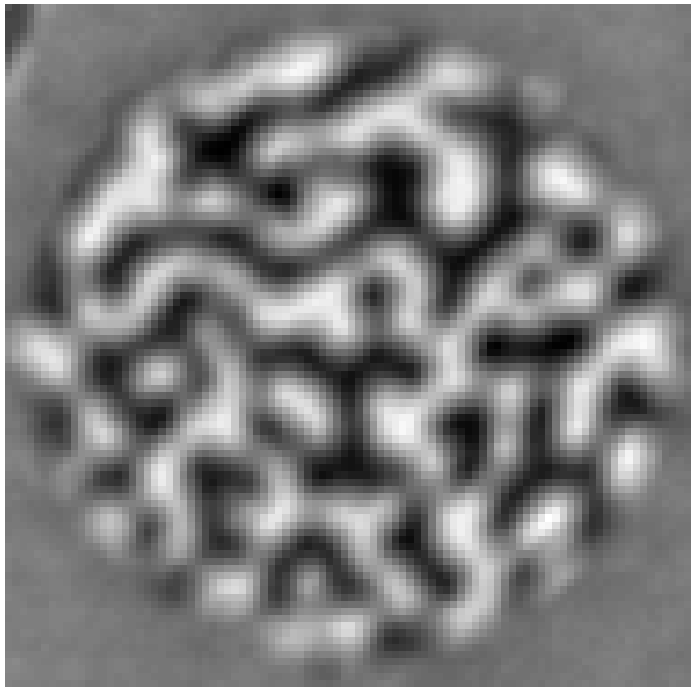

needs circular polarized x-rays

Method : S. Eisebitt et al. Nature 432, 885 (2004)
Resolution: L. M. Stadler et al. PRL, 100, 245503 (2008)

Photon Correlation Spectroscopy

Brownian Motion of 100 particles

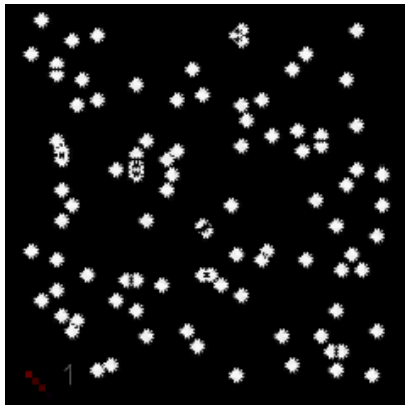

Diffraction Pattern

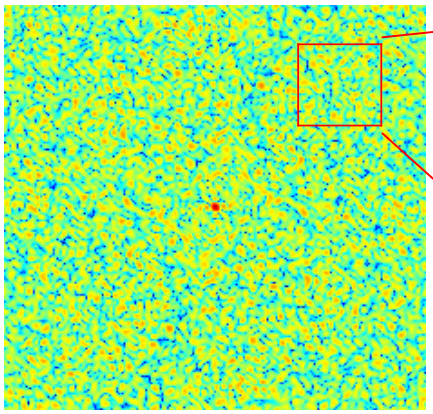

Speckles

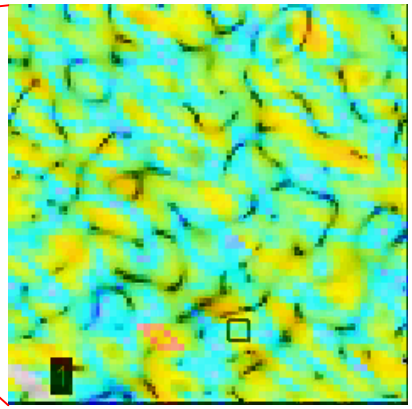

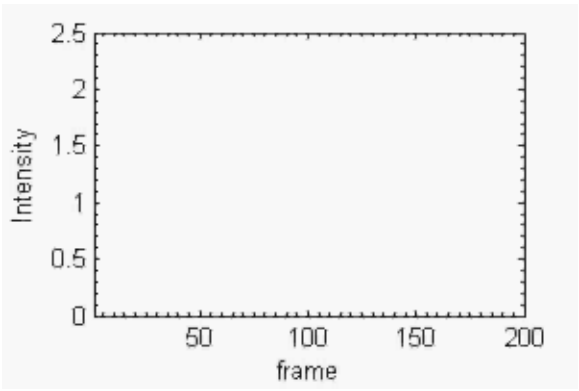

Intensity-intensity auto correlation

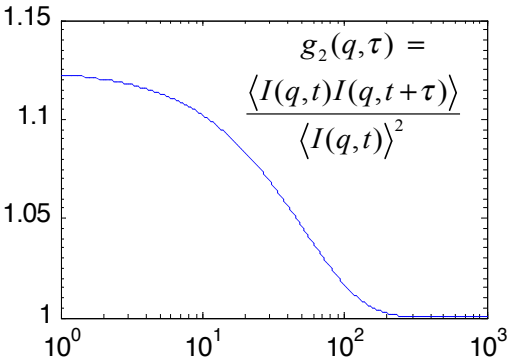

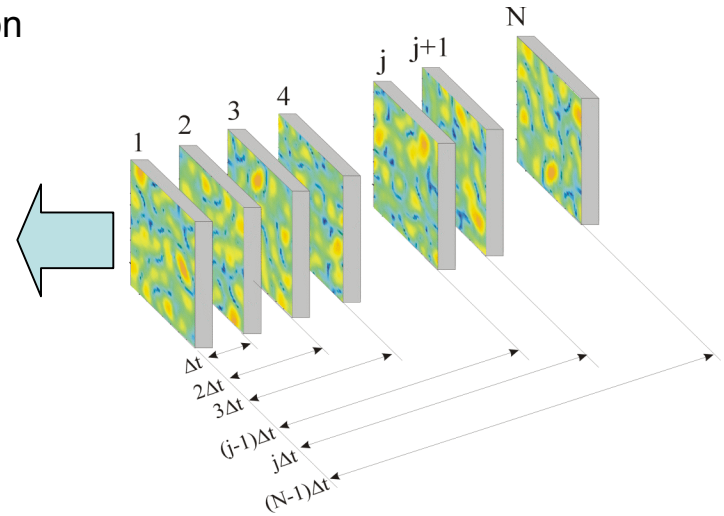

Photon Correlation Spectroscopy

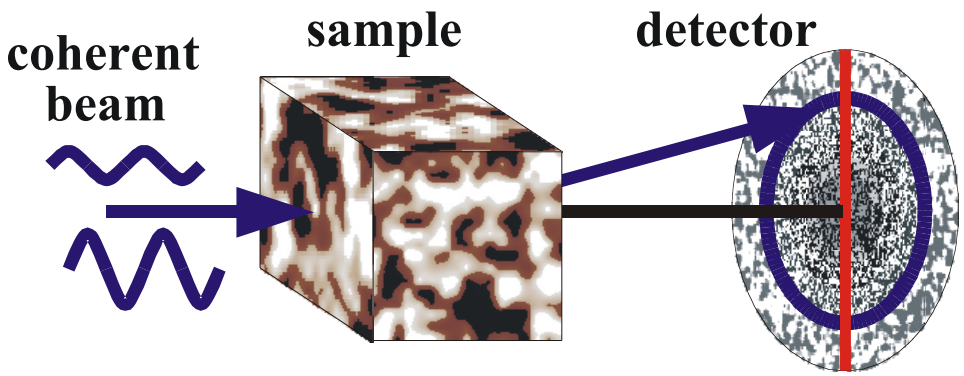

X-ray speckle pattern from a static silica aeroge

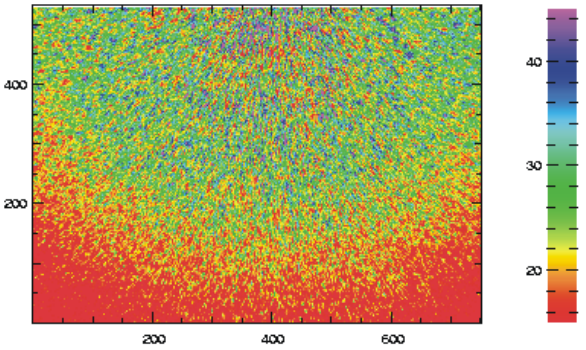

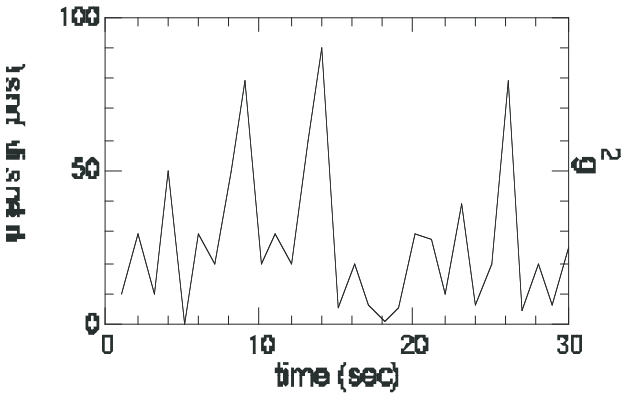

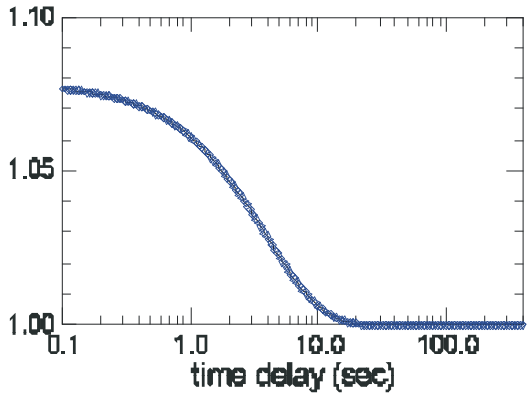

Siegert Reln.

$g_2(\mathbf{q},t) = |g_1(\mathbf{q},t)|^2$

$$g_2(q,t) = \frac{\langle I(q,t')I(q,t'+t)\rangle}{\langle I(q,t')\rangle^2}$$

$$g_2(t) = 1 + \beta \exp(-2\Gamma t)$$
$$= 1 + \beta \exp(-2t/\tau)$$

β:speckle contrast

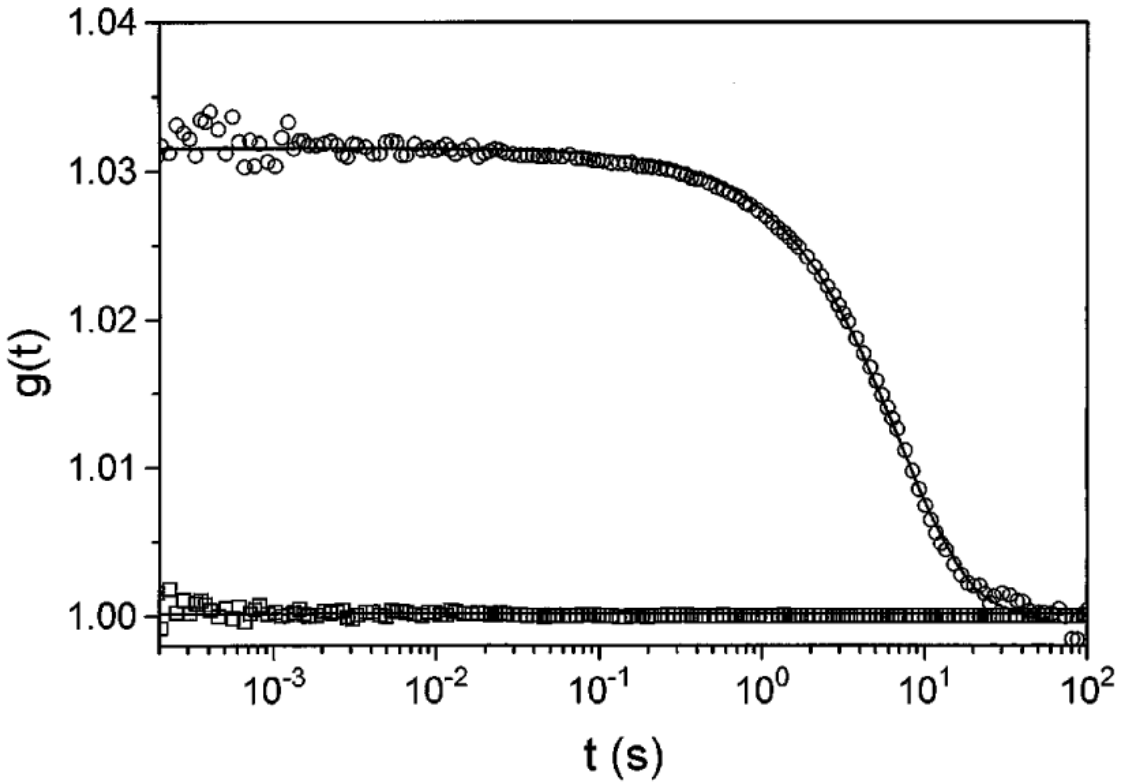

FIG. 3. Correlation function $g(t)$ measured for palladium colloid in glycerol at $q = 1.58 \times 10^{-3}$ Å^{-1} and $T = 279$ K. The solid line corresponds to a fit with an exponential decay. For comparison a correlation function measured for the incident beam is shown.

T. Thurn-Albrecht et al., PRL 1996

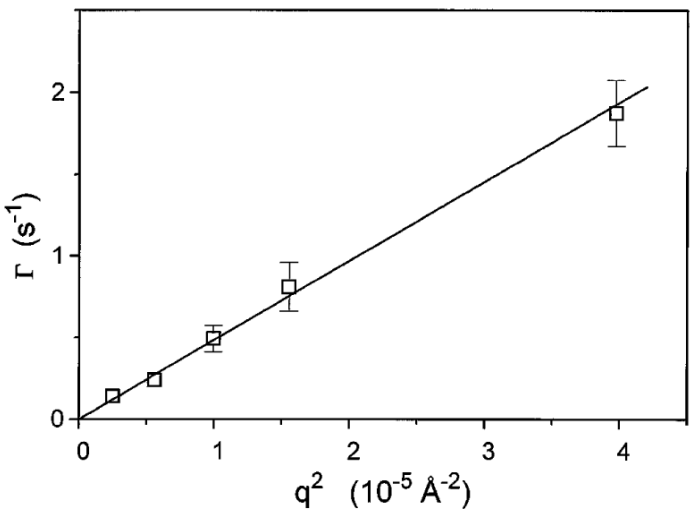

FIG. 4. Relaxation rates Γ determined from the correlation functions plotted vs q^2. The linear relationship confirms the diffusive nature of the process observed [Eq. (3)].

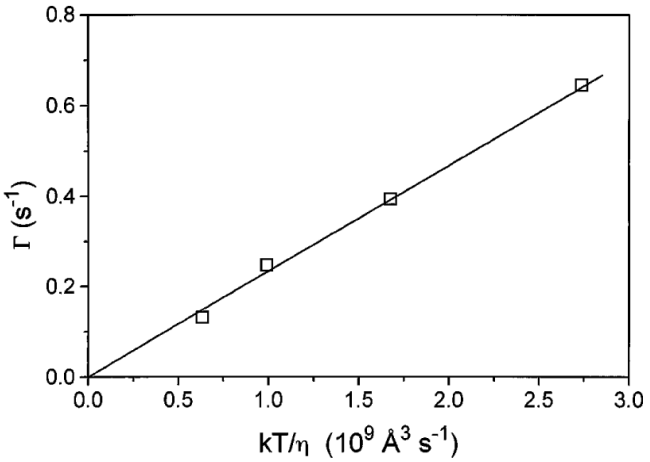

FIG. 5. Relaxation rates Γ determined from the correlation functions plotted vs kT/η. The linear dependence found in this representation is the expected behavior for a diffusion process [Eq. (4)].

SURFACE/INTERFACE DYNAMICS

Perfect & Imperfect „Mirrors“

Statistical Description of Surfaces

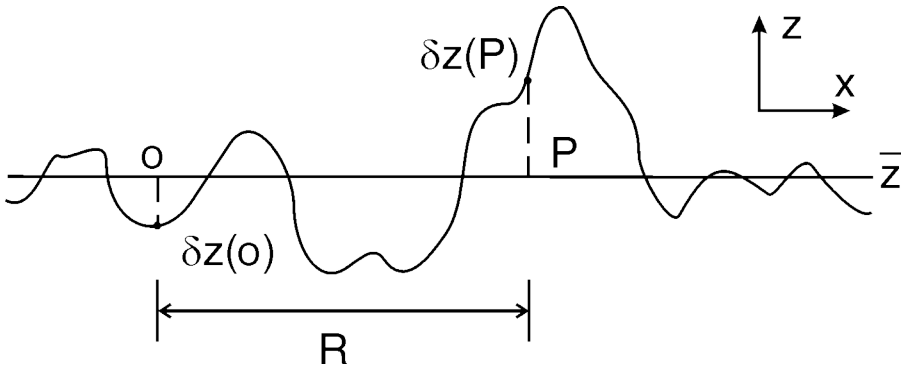

- Surface profile

$$z(\vec{r}_{\parallel}) = \bar{z} + \delta z(\vec{r}_{\parallel})$$

- Height-height correlation function for a homogeneous, isotropic and ergodic surface

$$C(R,\tau) = \langle \delta z(0) \delta z(R,\tau) \rangle$$

- FT[C(R)] measured in a surface scattering experiment

Intensity Autocorrelation

$$g_2(q,\tau) = \frac{\langle I(q,t)I(q,t+\tau)\rangle}{\langle I(q,t)\rangle^2}$$

$$g_2(q,\tau) = 1 + \beta e^{-2t/\tau}$$

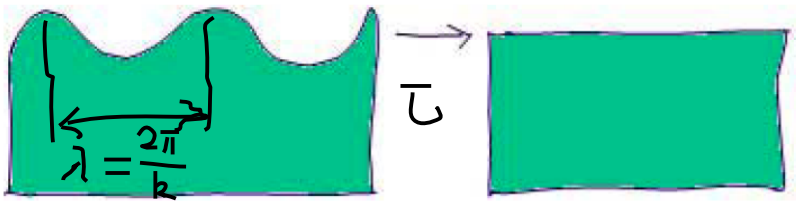

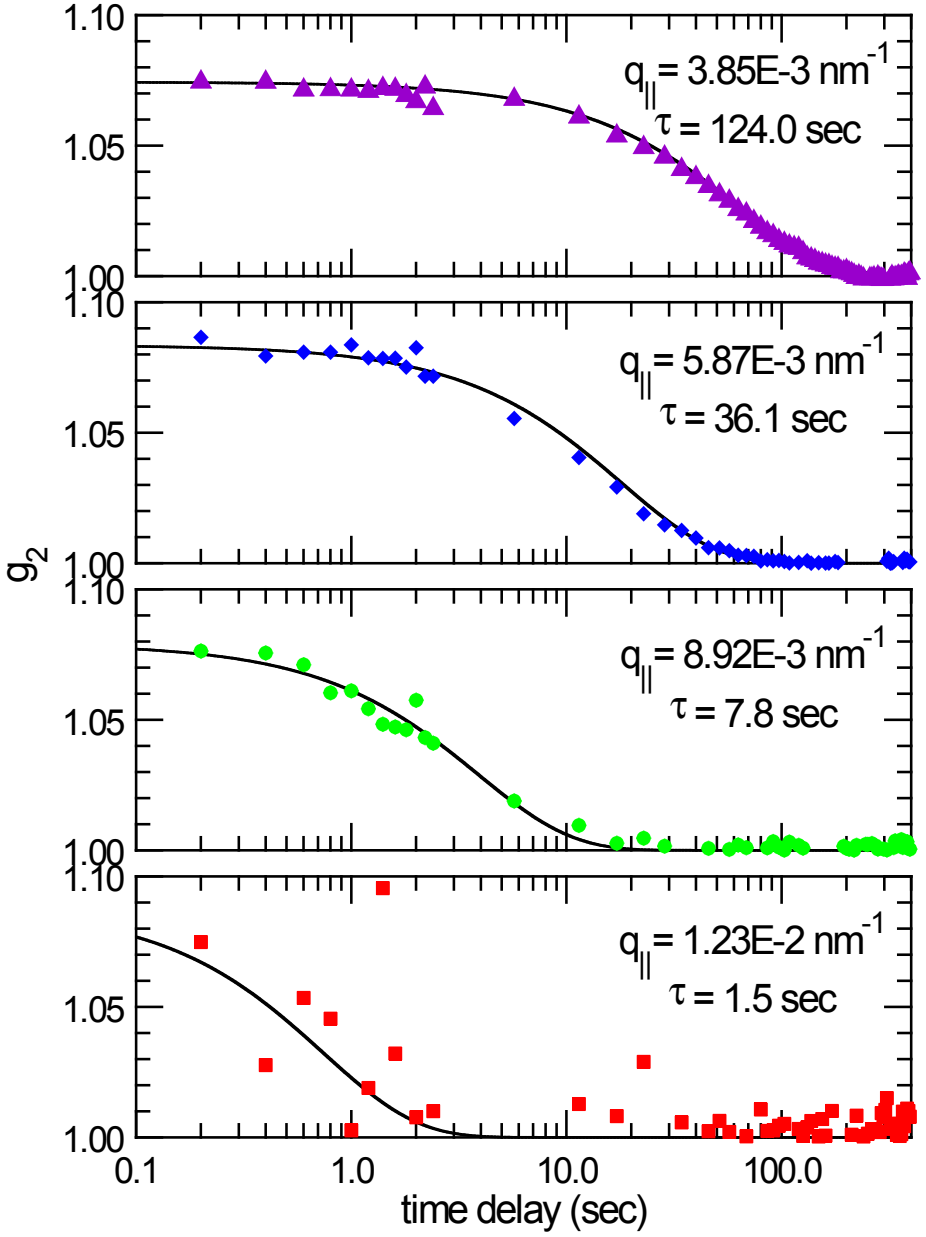

Hyunjung Kim, et.al., PRL 90, 68302 (2003)

Relaxation of Over-damped Capillary Wave (Thick Films h>>Rg)

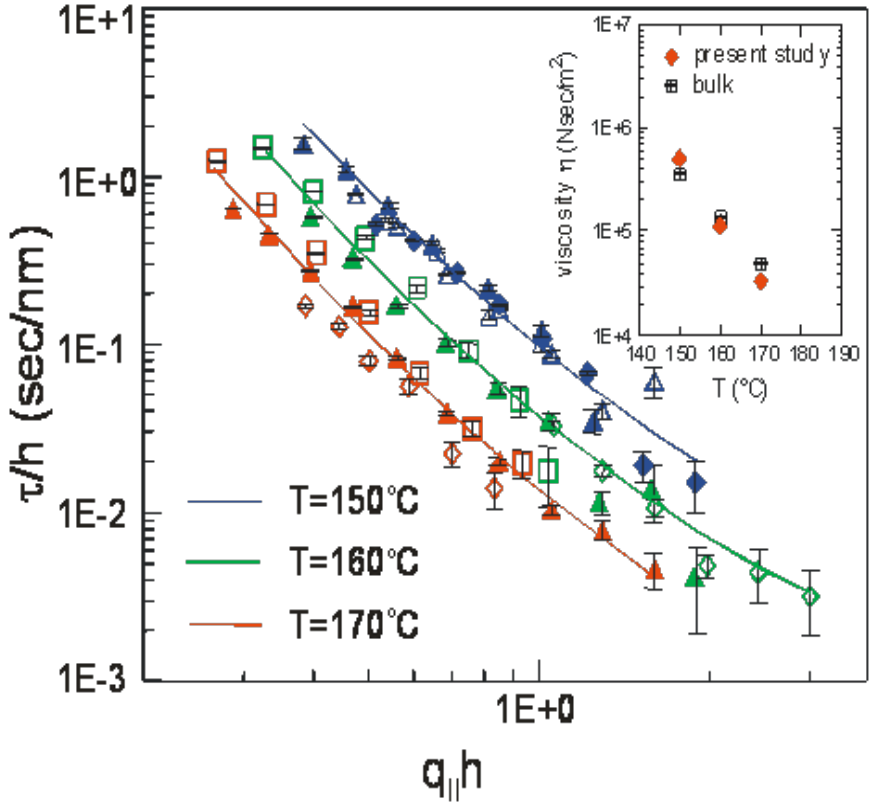

Over-damped relaxation time constants

Thickness scaling

$$\tau(q_{\parallel}) \cong 2\left(\frac{\eta}{\gamma}\right)\left(\frac{1}{q_{\parallel}}\right)\frac{[\cos(q_{\parallel}h)^2 + (q_{\parallel}h)^2]}{[\sinh(q_{\parallel}h)\cosh(q_{\parallel}h) - q_{\parallel}h]} \Rightarrow \frac{\tau}{h} = f(q_{\parallel}h)$$

η: shear viscosity
γ: surface tension
h: film thickness

- J. Jäckle, J. Phys: Condensed Matter 10, 7121 (1998)
- H. Kim, et al., Phys. Rev. Lett. 90, 68302 (2003)
- Z. Jiang, et al., Phys. Rev. E 74, 11603 (2006); M.L.Henle and A.J.levine, Phys. Rev. E 75,021604 (2007)

What happens as we lower the temperature to near Tg?

Z.Jiang et al. Phys. Rev. Lett. **101**, 246104 (2008)

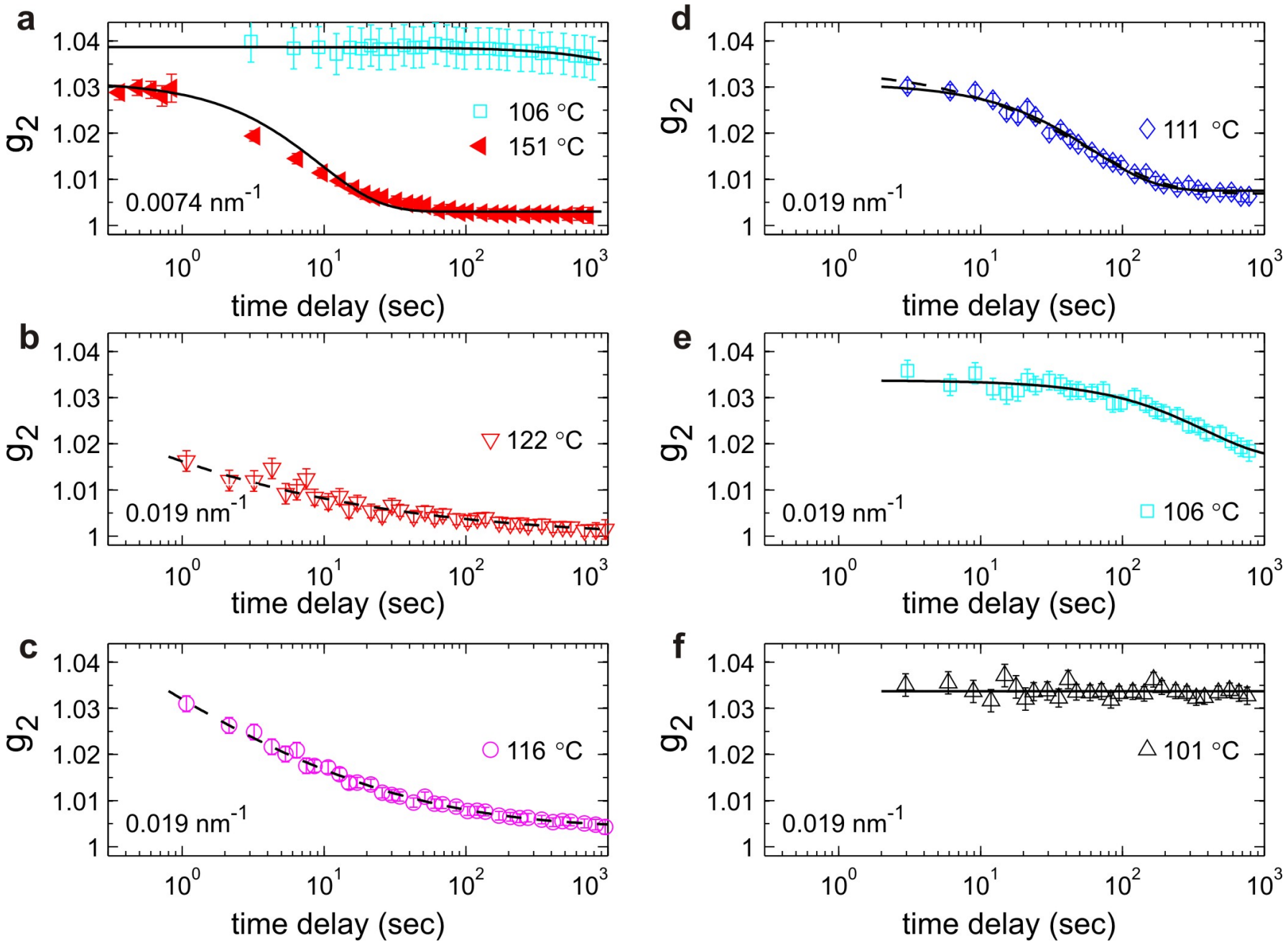
a
b
c
d
e
f
g_2
time delay (sec)
106 °C
151 °C
122 °C
116 °C
111 °C
101 °C
0.0074 nm^{-1}
0.019 nm^{-1}

“Apparent” Shear Viscosity

- Consistent with bulk values from rheological measurements at T>>Tg.
- Orders of magnitude less than bulk values and independent of Mw near Tg.
- Intersect with reptation theory ($\eta \propto Mw^{3.4}$) at Mw*
  - Mw* =Mc (Mc=31.2k g/mol: ***critical molecular weight for entanglement***).
- Same Mw* found at 106 ºC, where surface dynamics are 7 times slower.

$$\eta = \lim_{\omega \to 0} \frac{G''(\omega)}{\omega}$$

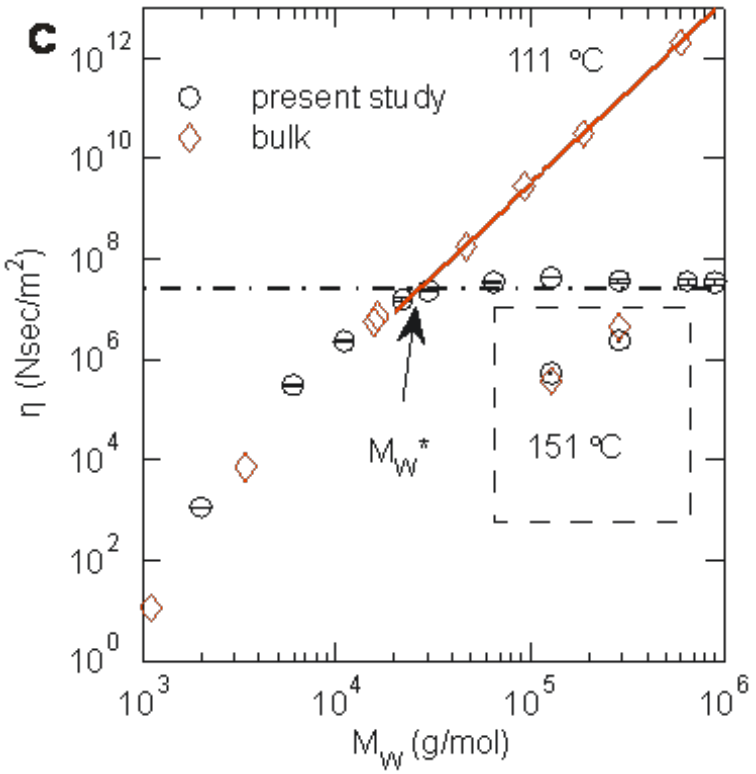

Z.Jiang et al., PRL 2008

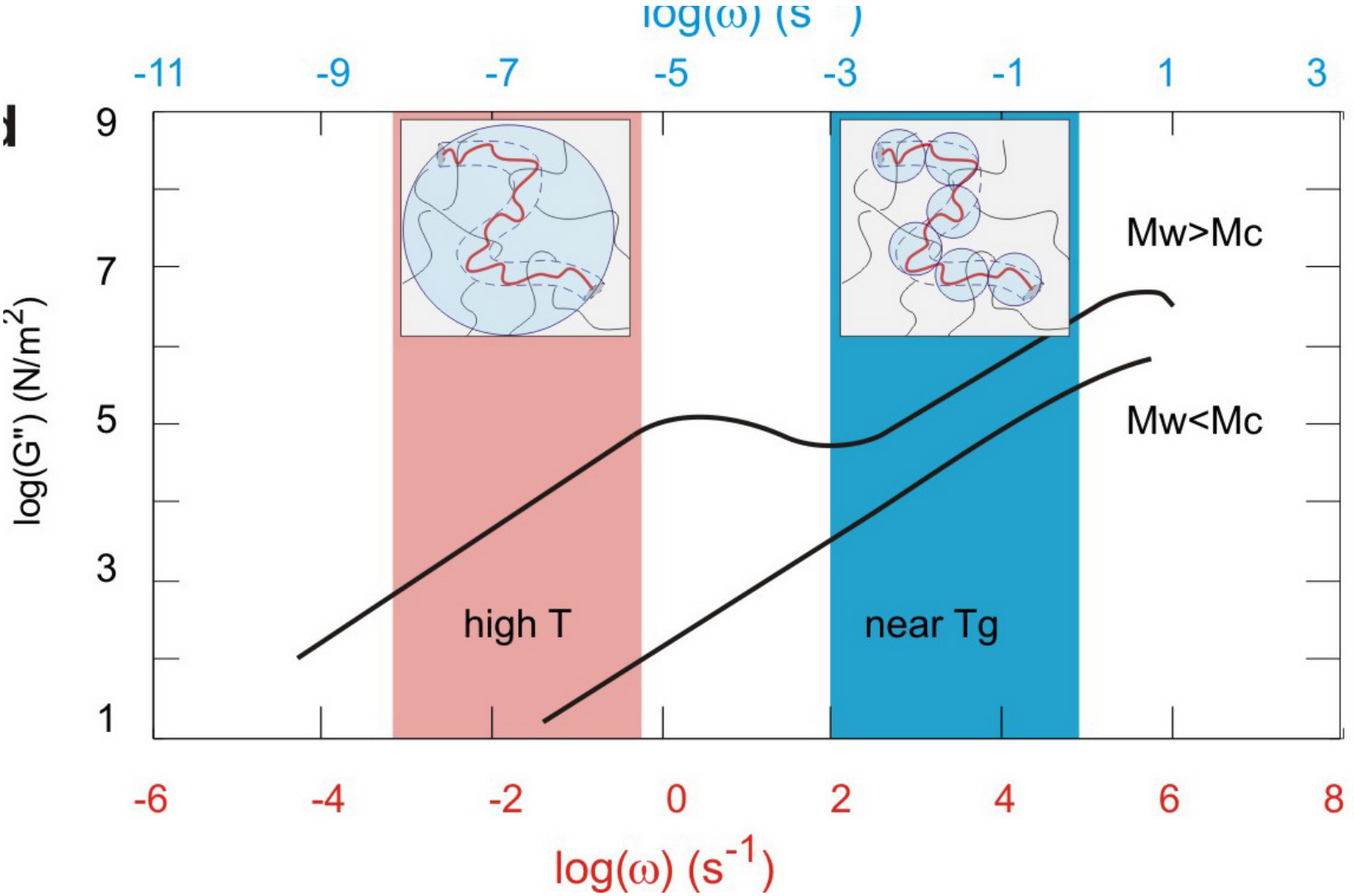
log(ω) (s
-11
-9
-7
-5
-3
-1
1
3
9
7
5
3
1
log(G") (N/m2)
Mw>Mc
Mw<Mc
high T
near Tg
-6
-4
-2
0
2
4
6
8
log(ω) (s-1)

Incoherent SAXS

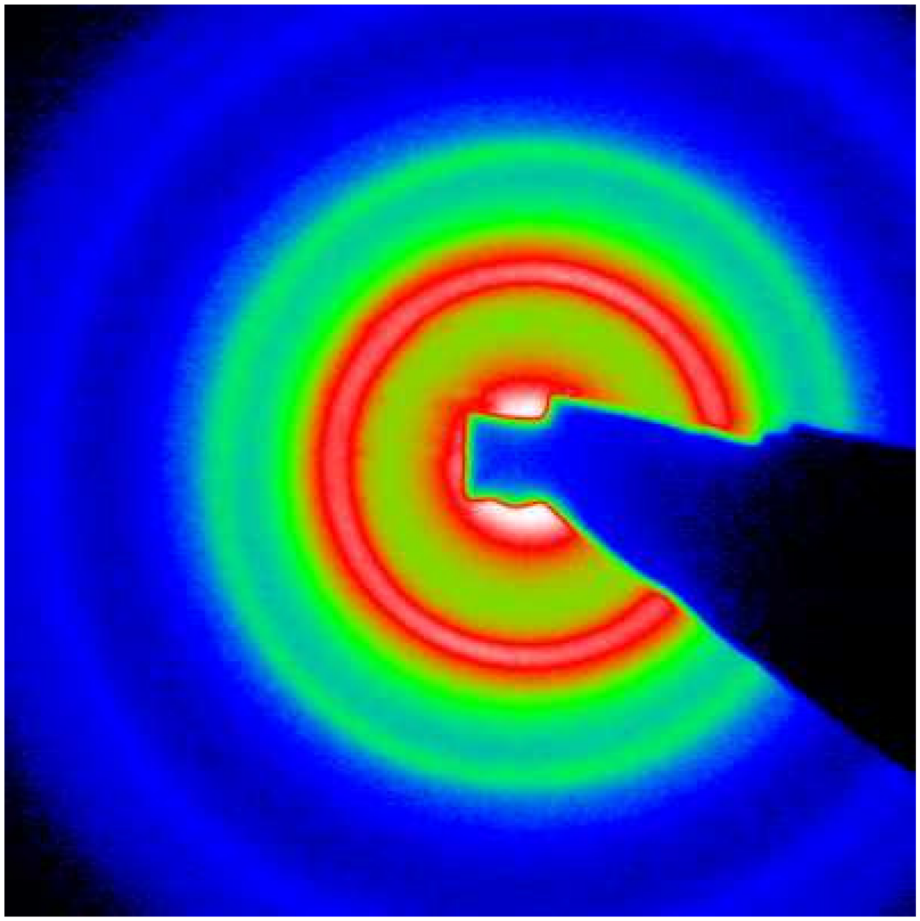

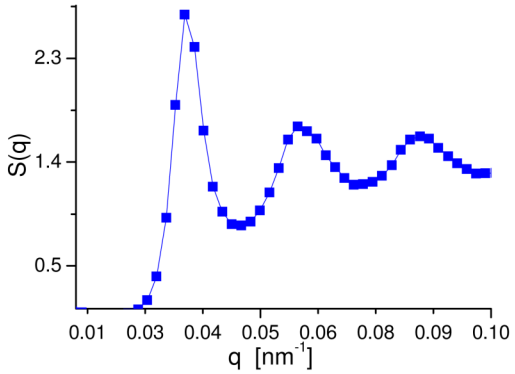

ensemble averaged structure factor

$$< S(Q) >= 1 + n_0 \int (g(r) - 1) e^{iQr} dr$$

radial distribution function

$$g(r) = 4\pi r^2 n_0^{-2} < \rho(0)\rho(r) >$$

information on local symmetries is lost

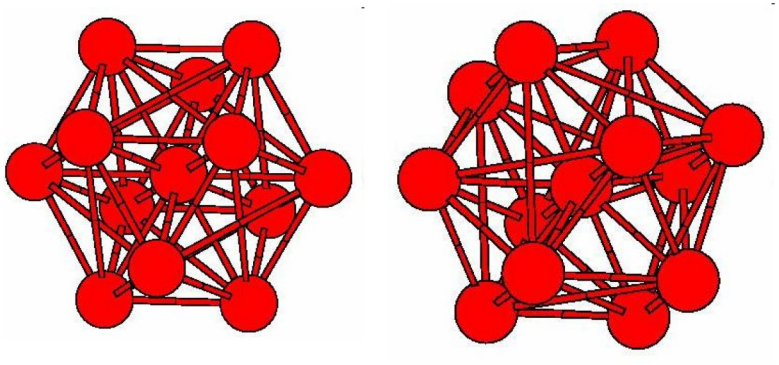

fcc and hcp structures can fill up space
and form crystals

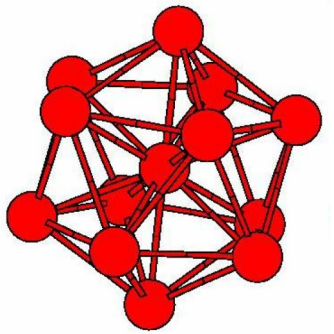

icosahedral structures can not fill space
but may be energetically favored in liquids
“locally favored structures (lsf)”

F. C. Frank, Proc. R. Soc. London A 215, 43 (1952).
P. J. Steinhardt, D. R. Nelson, and M. Ronchetti, Phys. Rev. B 28, 784 (1983)

Hard sphere systems – speckle pattern

P.Wochner et al.

PNAS 2009

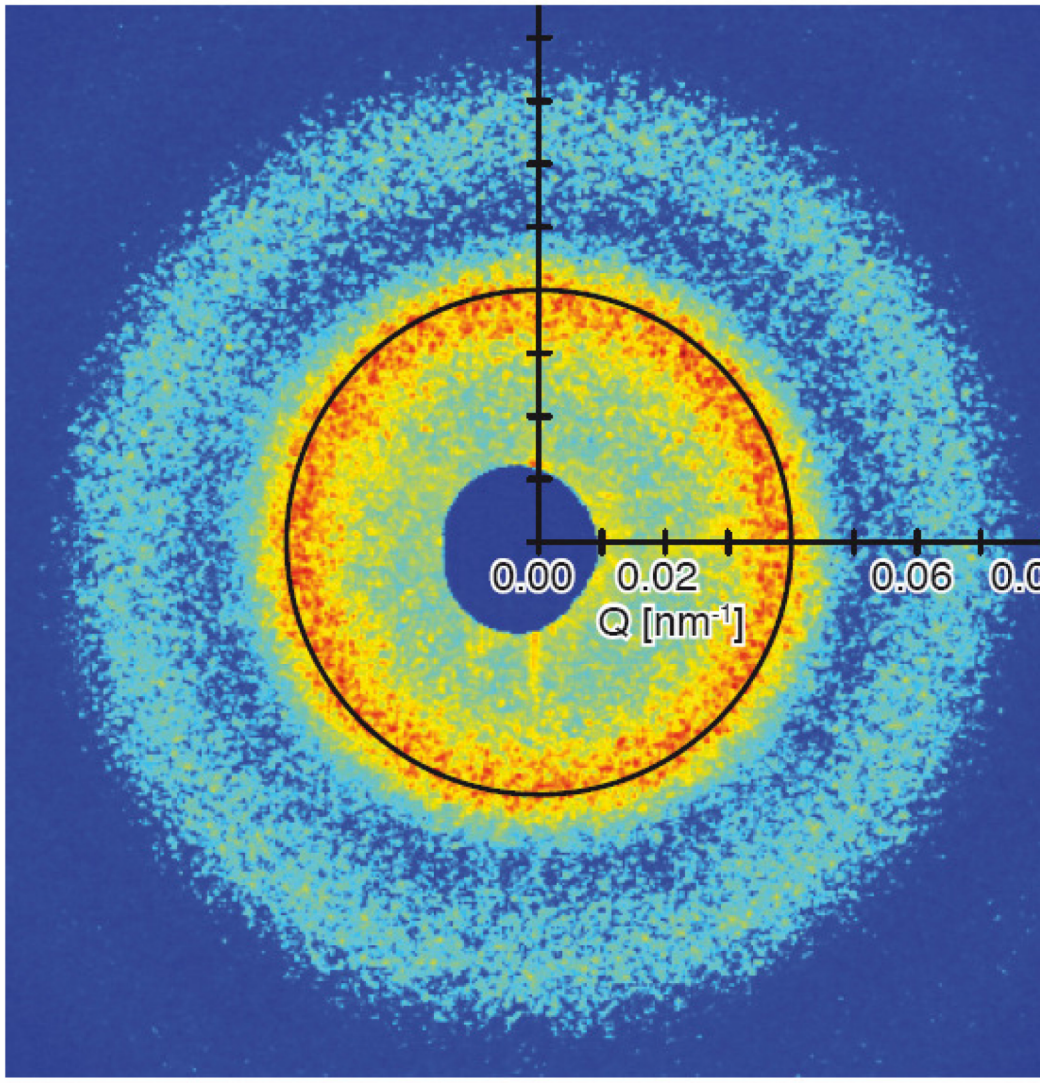

5-fold symmetry present in all hard sphere systems

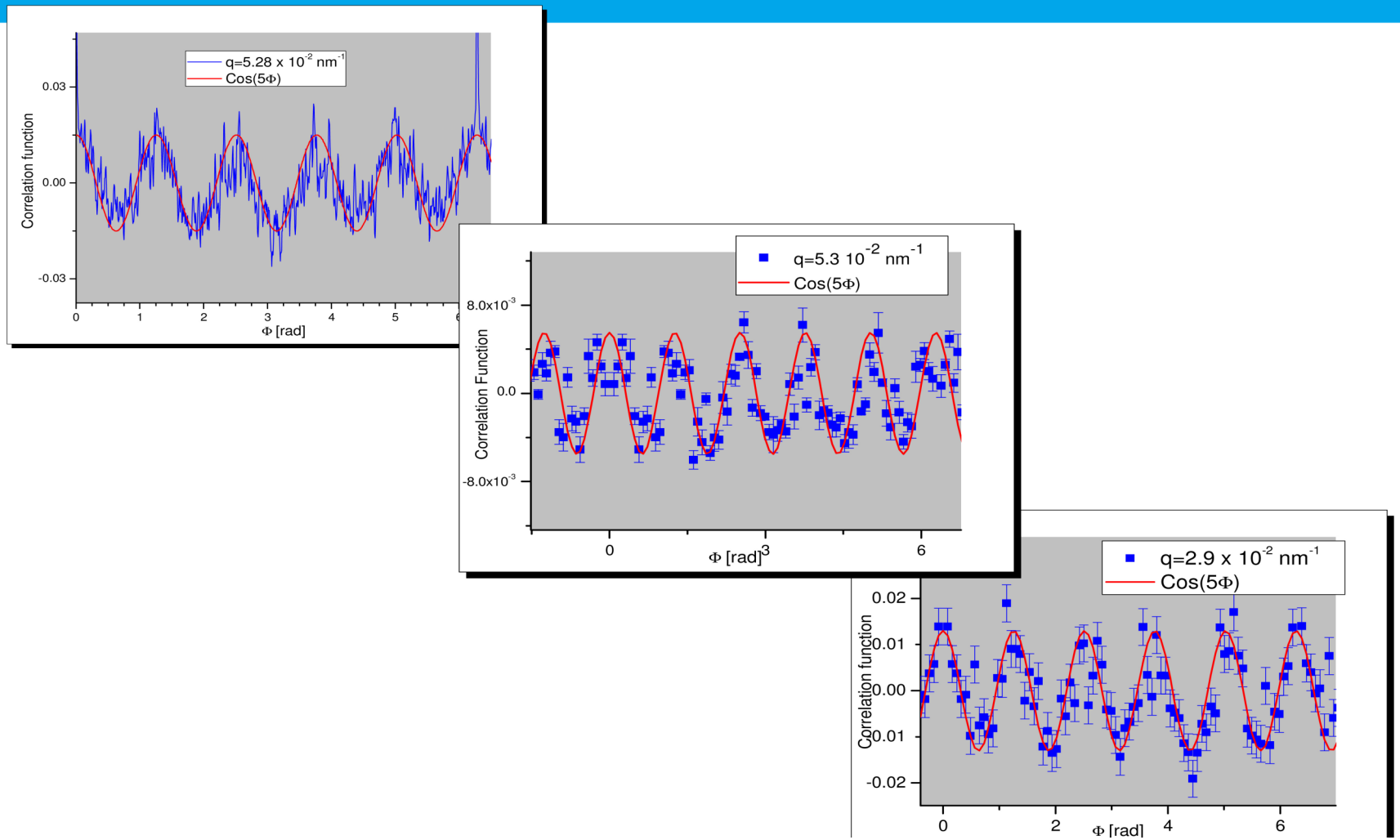

XPCS on Magnetic System – Provides Information about Domain Dynamics

- **XPCS can study slow dynamics ranging from milliseconds to hours → magnetic domain motion or critical slowing down.**

- **Limited XPCS work in magnetic system has been reported.**
  Shpyrko *et. al* – Nature **447**, 68 (2007) → ***Study of AF Cr***
  Seu *et. al* – PRB **82**, 012404 (2010) → ***Study of ultrathin Co***
  Konings *et. al* – PRL **106**, 077402 (2011) → ***Study of Ho***

A suitable system needs:

a. **Reflection geometry**
b. **Not too small in Q – contamination by charge roughness scattering**
c. **Not too large in Q – would not be able to reach with soft x-rays.**

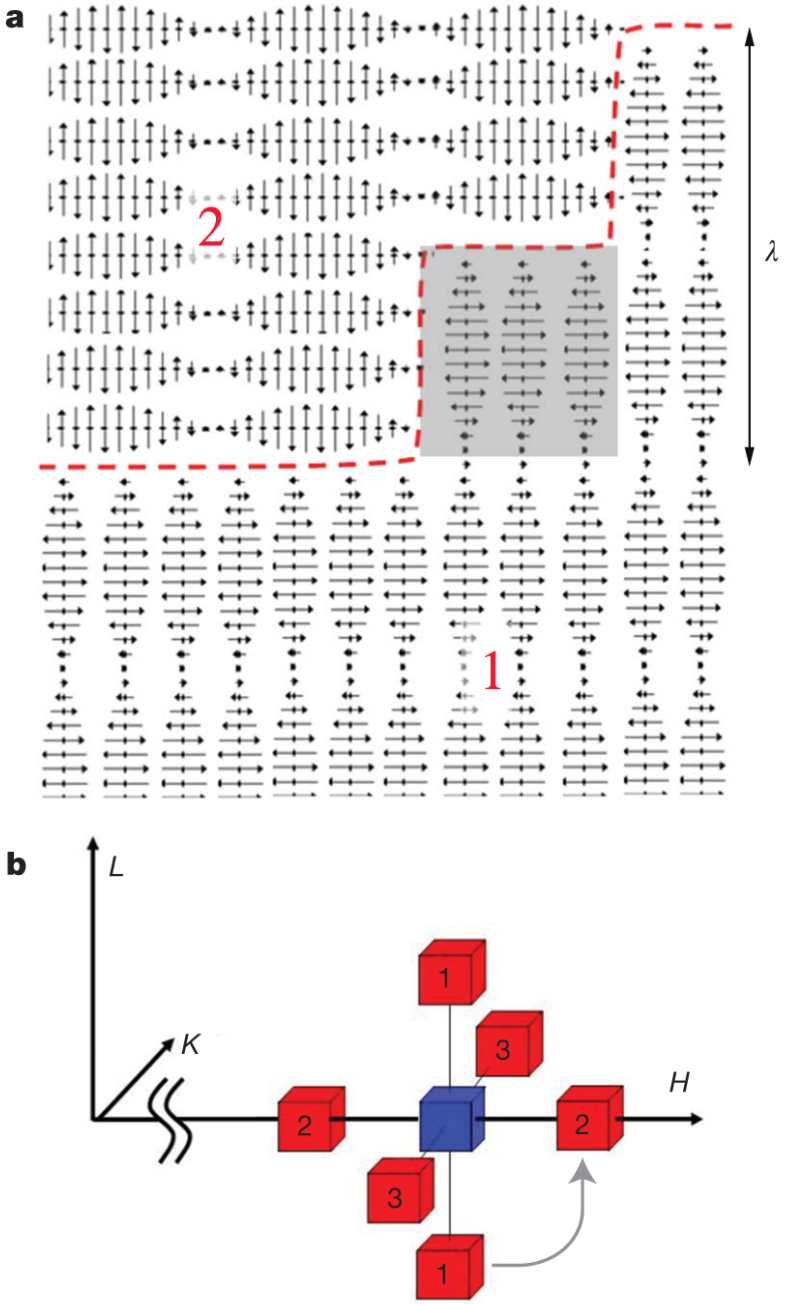
a
2
1
λ
b
L
K
H
1
3
2
2
3
1

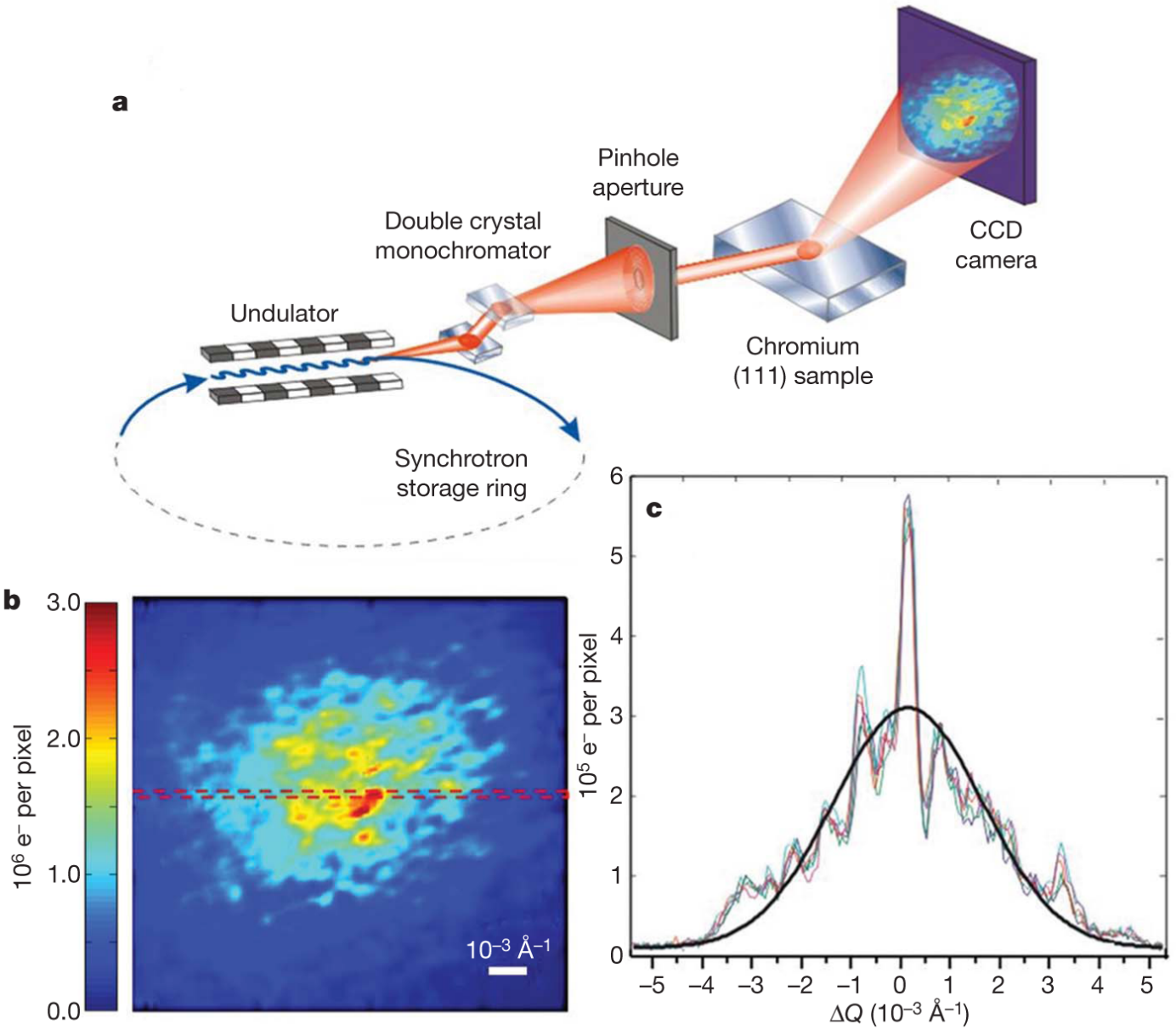
a
Pinhole
aperture
Double crystal
monochromator
CCD
camera
Undulator
Chromium
(111) sample
Synchrotron
storage ring
b
3.0
2.0
1.0
0.0
10⁶ e⁻ per pixel
10⁻³ Å⁻¹
c
6
5
4
3
2
1
0
10⁵ e⁻ per pixel
–5 –4 –3 –2 –1 0 1 2 3 4 5
ΔQ (10⁻³ Å⁻¹)

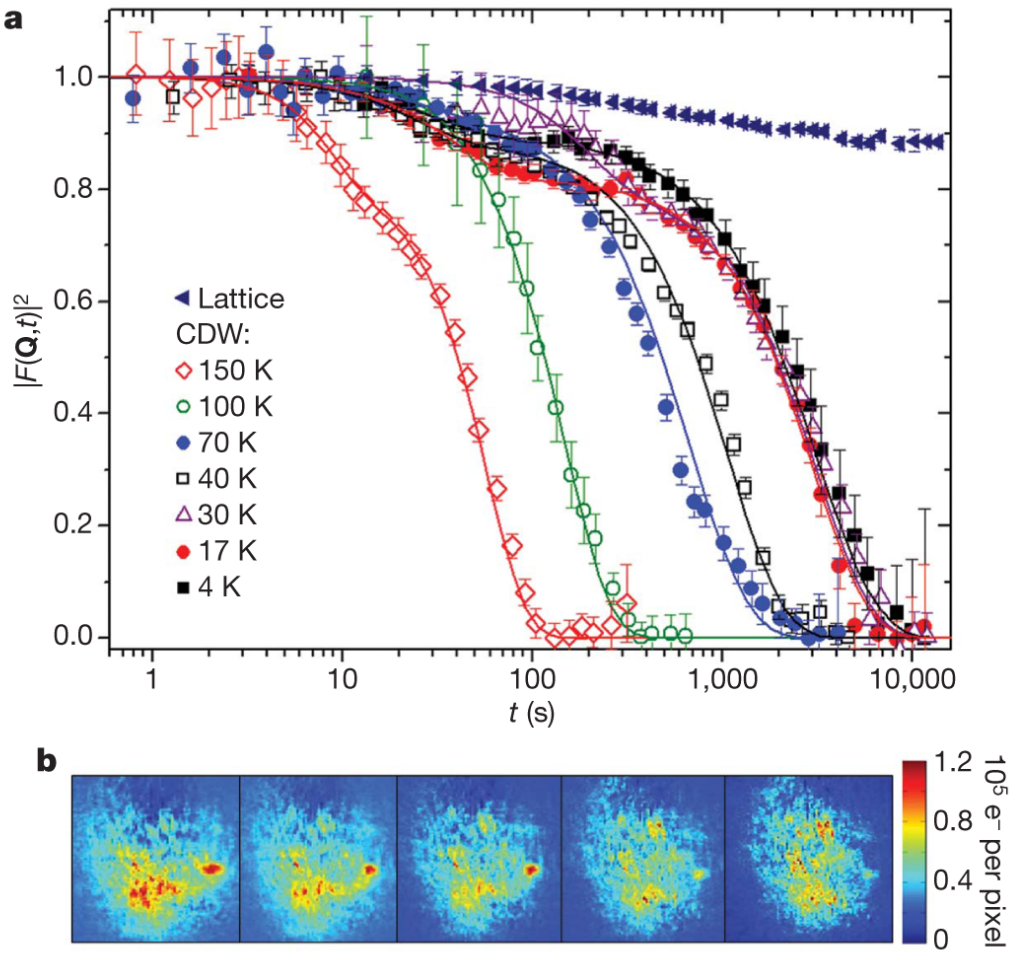

Figure 3 | Autocorrelation of speckle images. **a**, Intensity autocorrelation data for the [200] lattice Bragg peak, as well as for the CDW superlattice $[2-2\delta, 0, 0]$ peak, at temperatures T (in K) 150, 100, 70, 40, 30, 17 and 4. Error bars, standard deviation calculated for a region of interest within the CCD typically containing $n = 4 \times 10^4$ pixels. Two distinct timescales are clearly present in the CDW autocorrelation function. Solid lines represent theoretical fits to the data. See text for further details. **b**, Time sequence of CDW speckle pattern evolution at 17 K. Subsequent images are taken 1,000 s apart; each image is 10^{-2} Å$^{-1} \times 10^{-2}$ Å^{-1}.

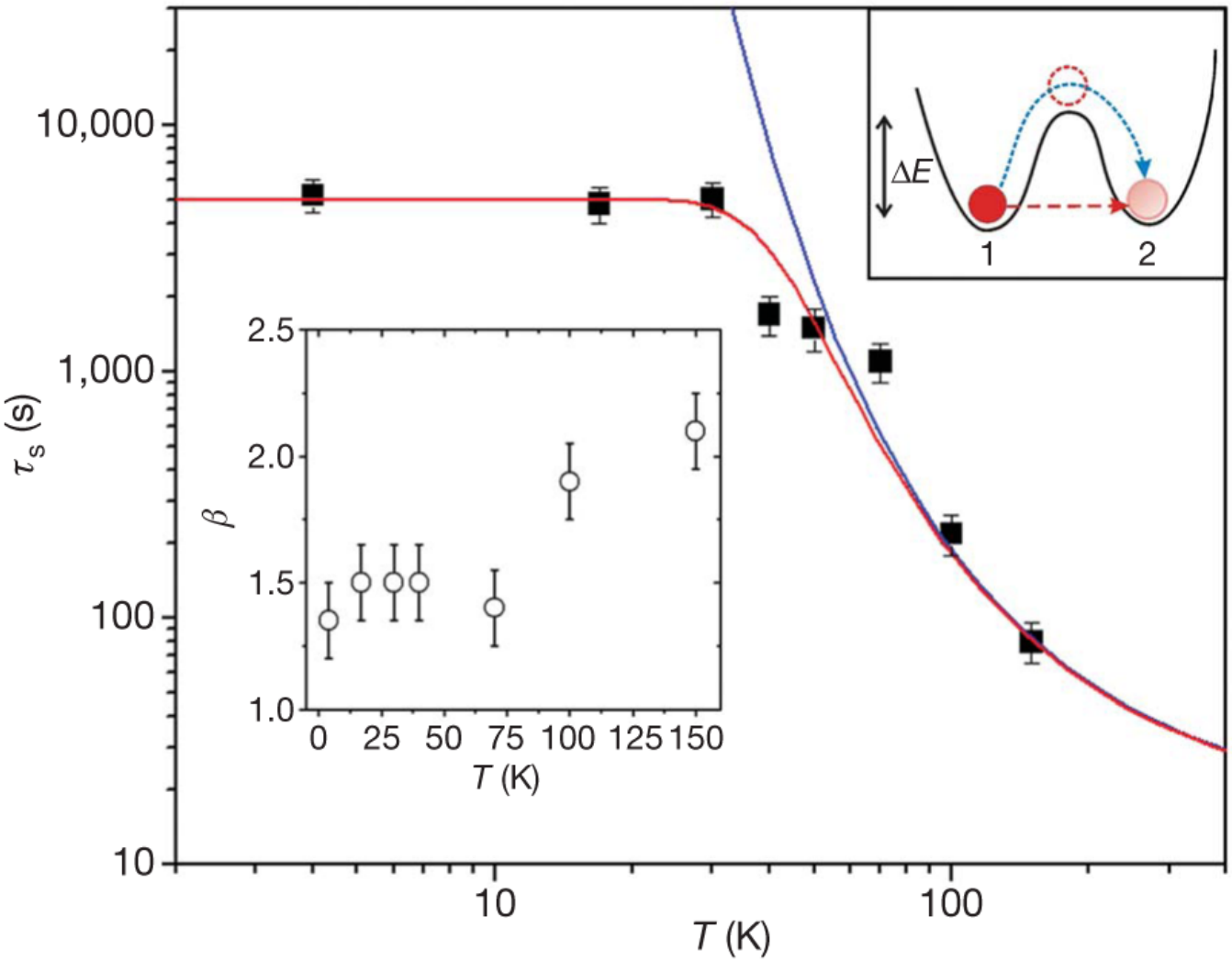

ure 4 | Temperature-dependent domain wall dynamics. Main plot

The Sample: Y/Dy/Y

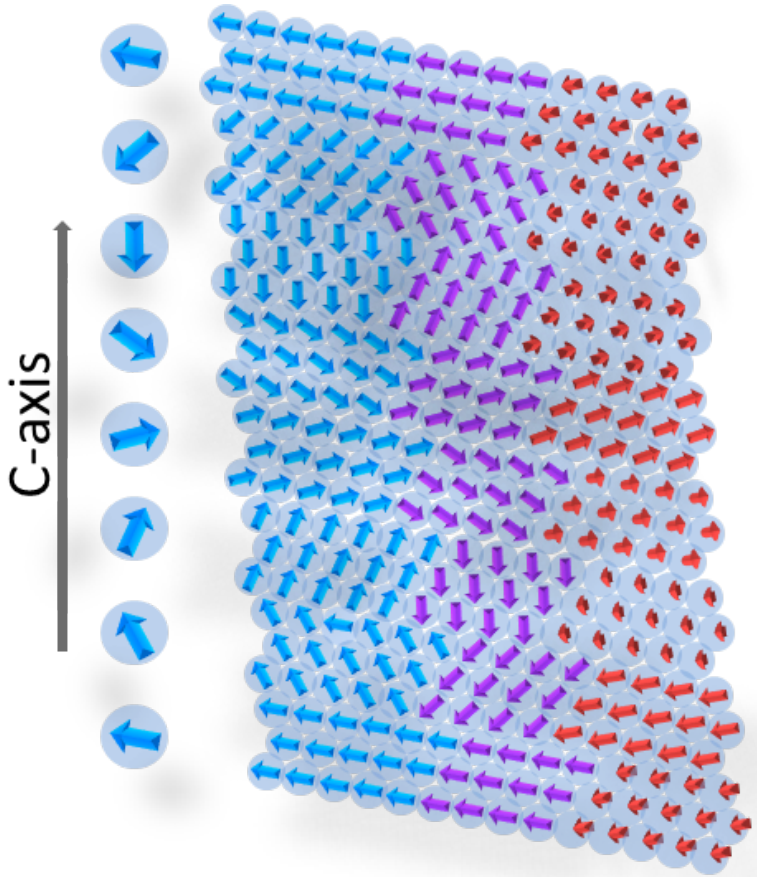

8ML spiral, turning angle 45°

- Hexagonal lattice. Spiral antiferromagnetic phase between T_C (~85K) and T_N (180K).
- Magnetic scattering is enhanced at resonant edge (M_5 1305eV) and the magnetic diffraction peak can be seen.
- Domains are formed in single layer, with different chirality and defects etc.

Temperature Dependence of the Spiral Antiferromagnetic Bragg Peak

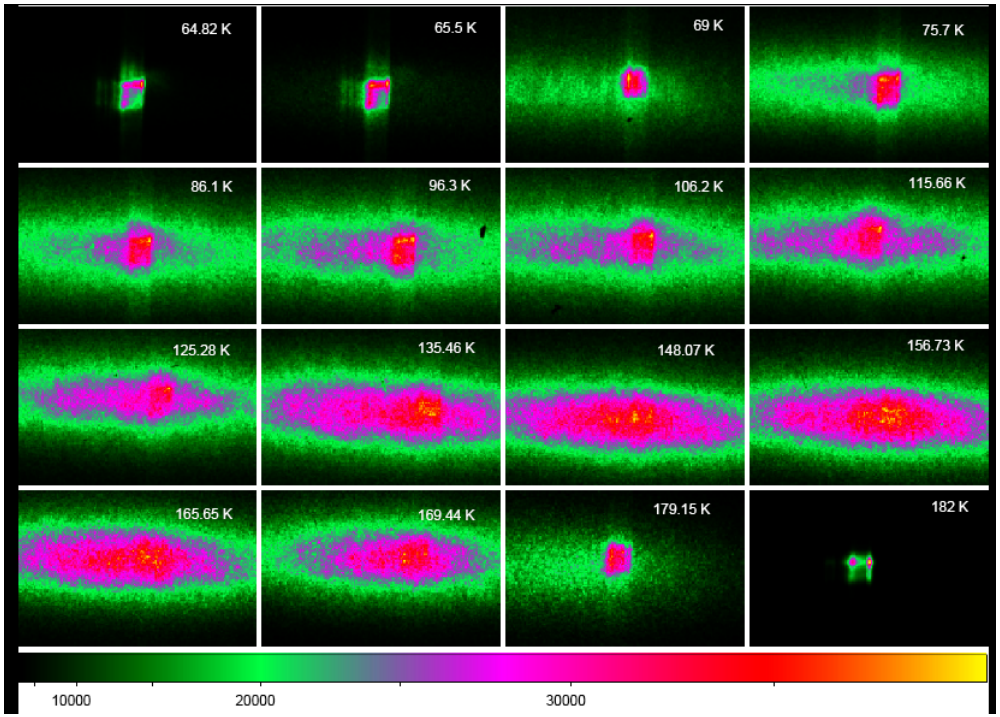

Y/Dy(500nm)/Y trilayer
(0,0,0.2) Bragg peak

- Reported T_C is about 85K, but magnetic diffraction peak does not disappear until 65K.
- Diffraction peak vanishes at reported T_N = 180K.

Temperature Dependence of the Turn Angle

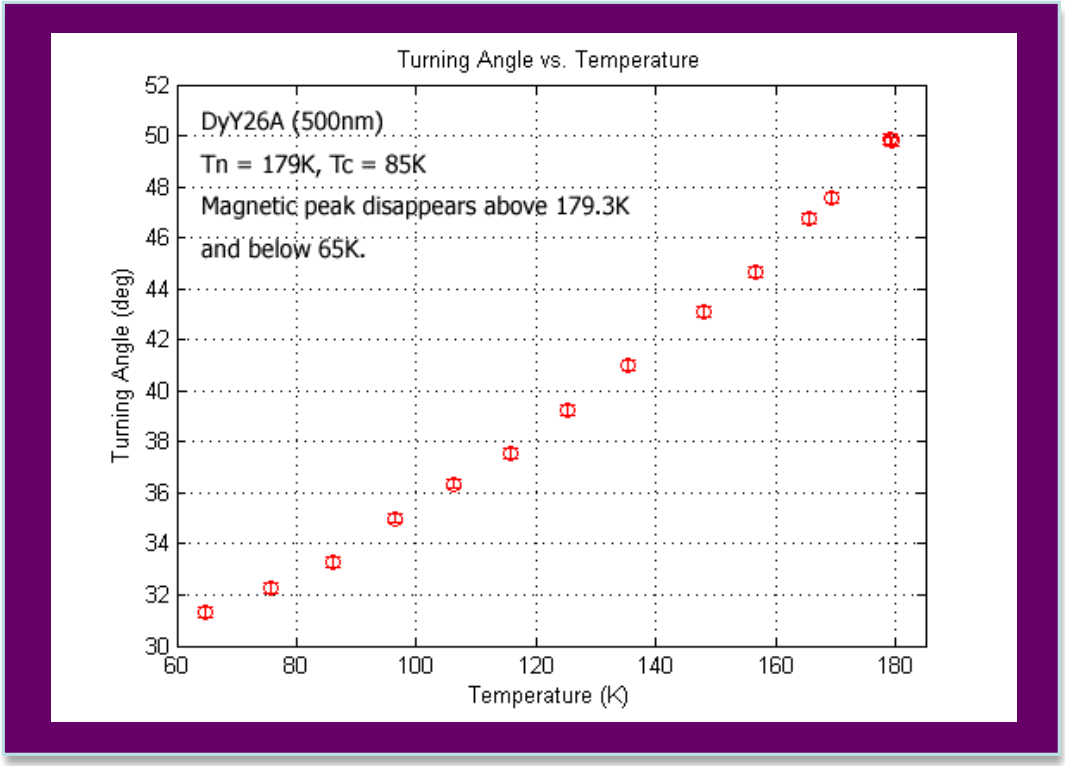

- Turn angle changes from 50 degrees at 180K to 31 degrees to 64K – change of AF Bragg plane distance.

Temperature Dependence of Correlation Length

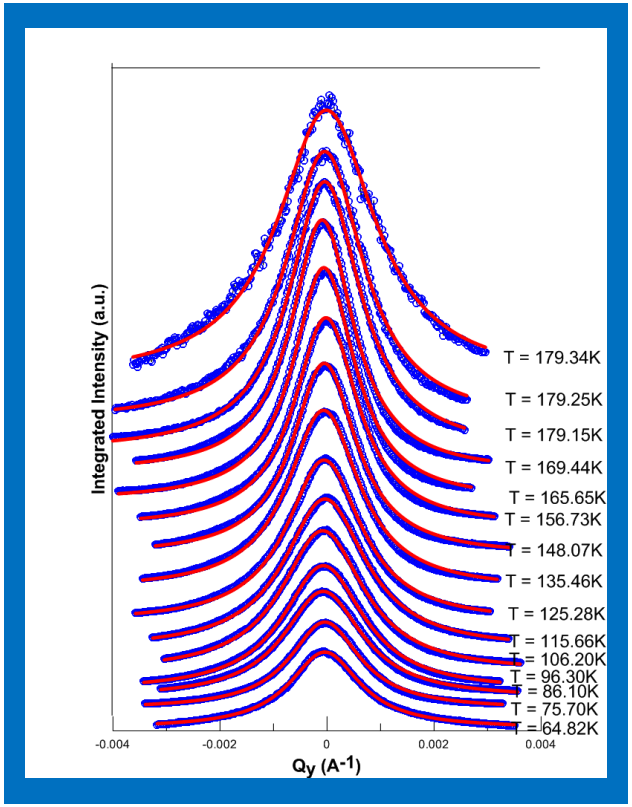

Single Lorentzian fit to the magnetic Bragg peak.

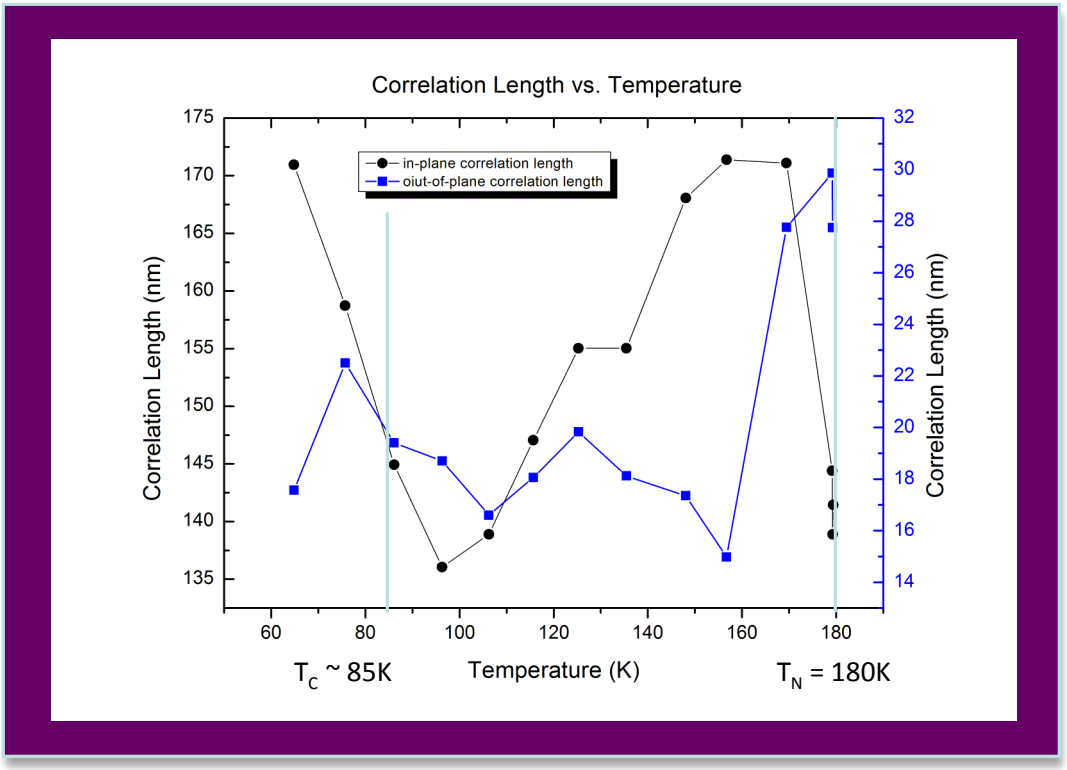

Static Speckles

T = 77K (near T_C)

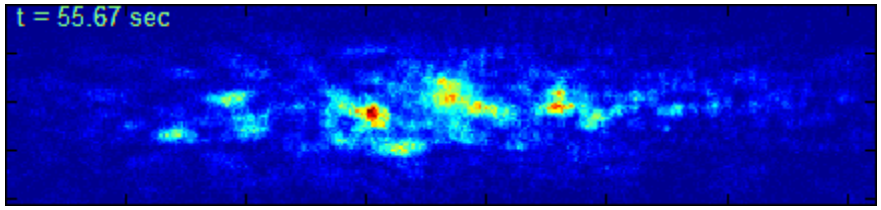

T = 141K

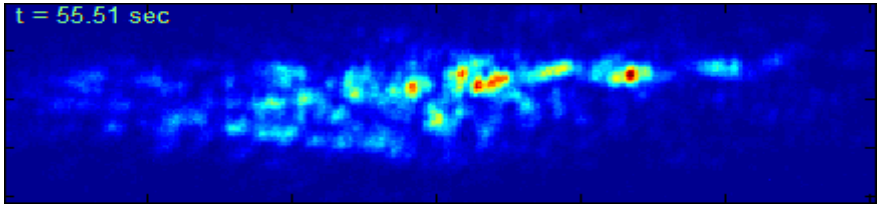

- From temperature near T_C (1^{st} order phase transition) all the way to near T_N, the speckles are static. No dynamics observed.

Dynamics near T_N

T = 170K

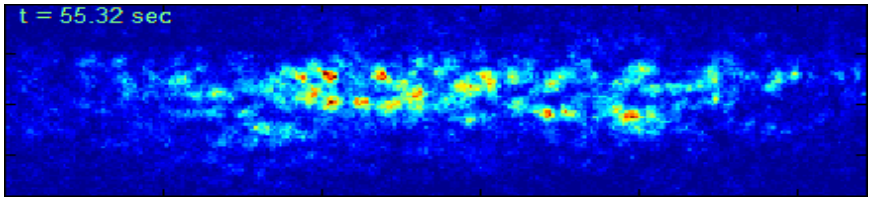

T = 178.4K

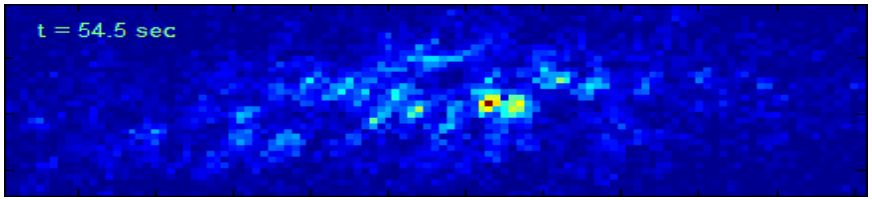

T = 179.0K

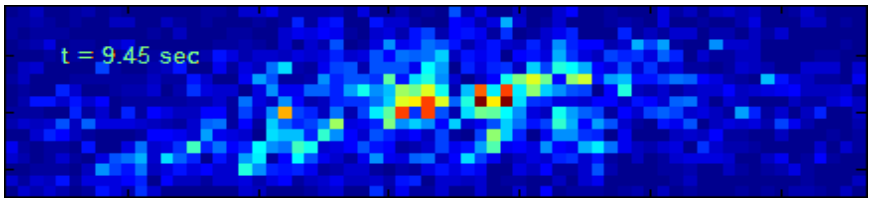

XPCS

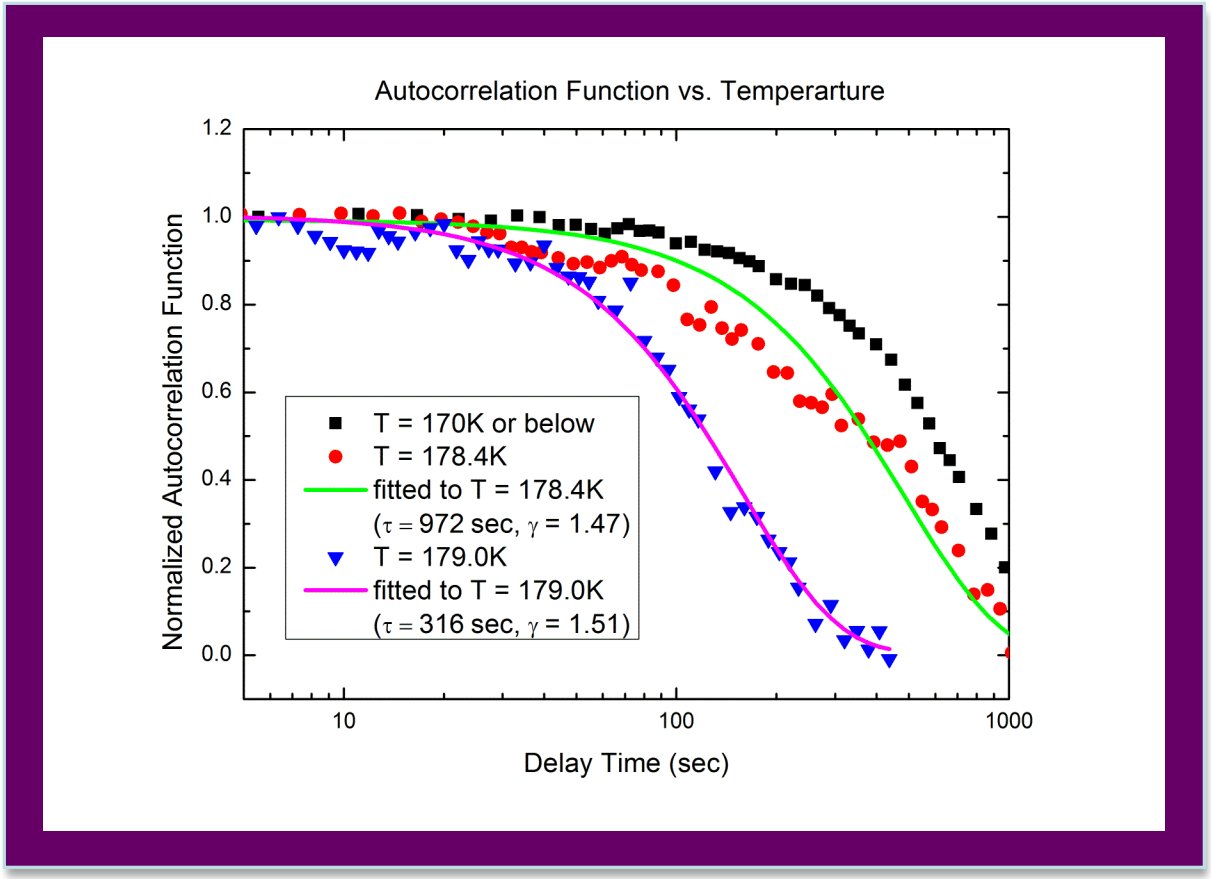
Autocorrelation Function vs. Temperarture
Normalized Autocorrelation Function
1.2
1.0
0.8
0.6
0.4
0.2
0.0
10
100
1000
Delay Time (sec)
T = 170K or below
T = 178.4K
fitted to T = 178.4K
(τ = 972 sec, γ = 1.47)
T = 179.0K
fitted to T = 179.0K
(τ = 316 sec, γ = 1.51)

Diffraction Imaging

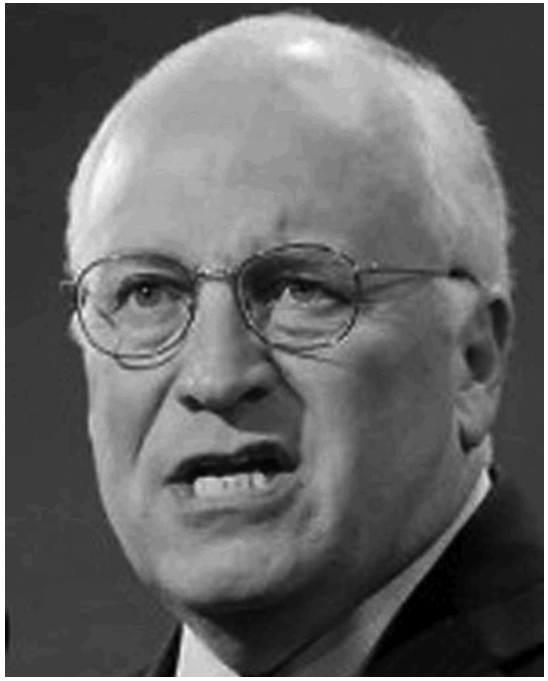

The “Phase Problem”

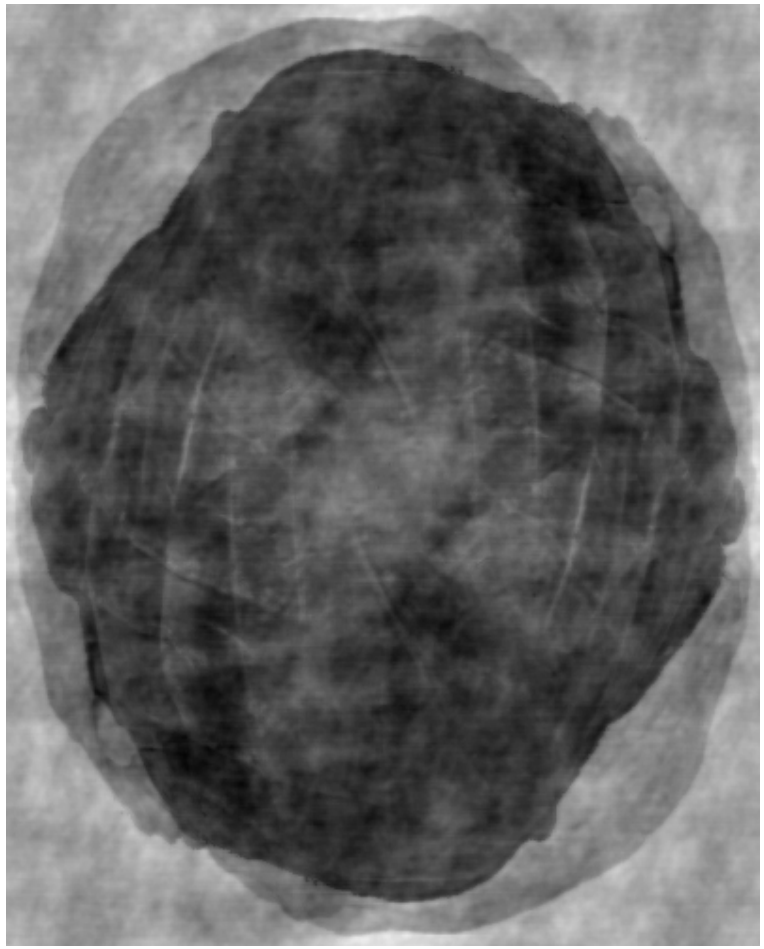

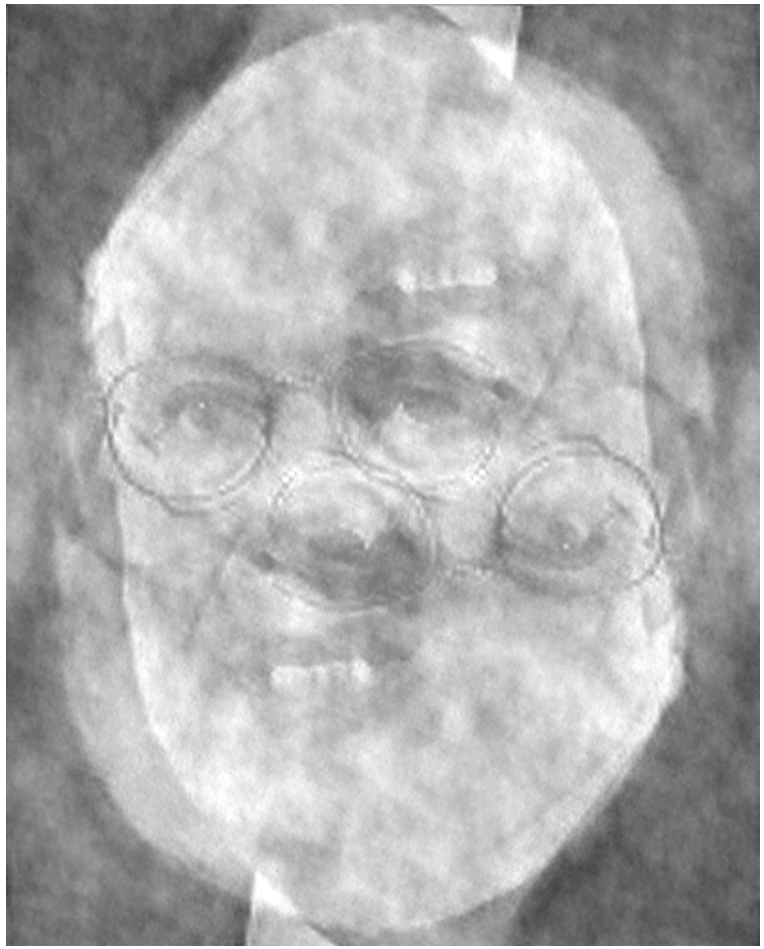

Miao, Charalambous, Kirz, Sayre, *Nature* **400**, 342 (1999).

λ=1.8 nm
soft x-ray
diffraction
pattern

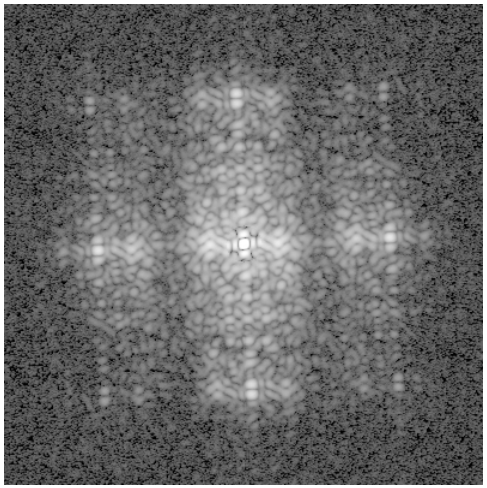

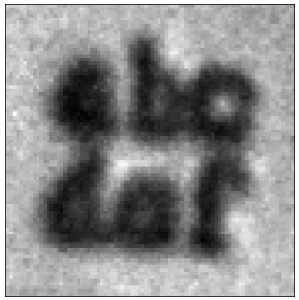

Low angle data
From optical
micrograph

Scanning
electron
micrograph
of object

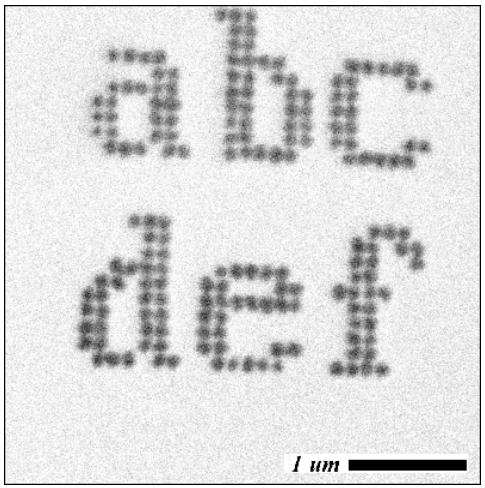

Image reconstructed
from diffraction
pattern (θ_{max}
corresponds to 80
nm). Assumed
positivity

Reconstruction

Equations can still not be solved analytically

Fienup iterative algorithm

Reciprocal space Real space

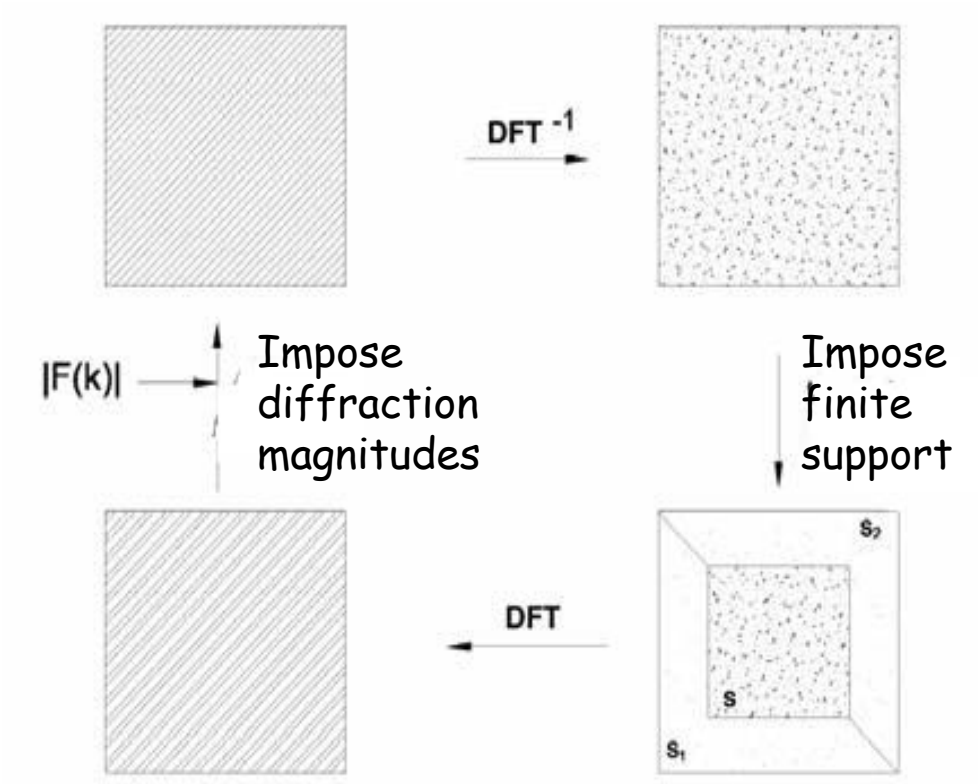

•Positivity of electron density helps!

Successful reconstruction of image from soft X-ray speckle alone.

SEM Image

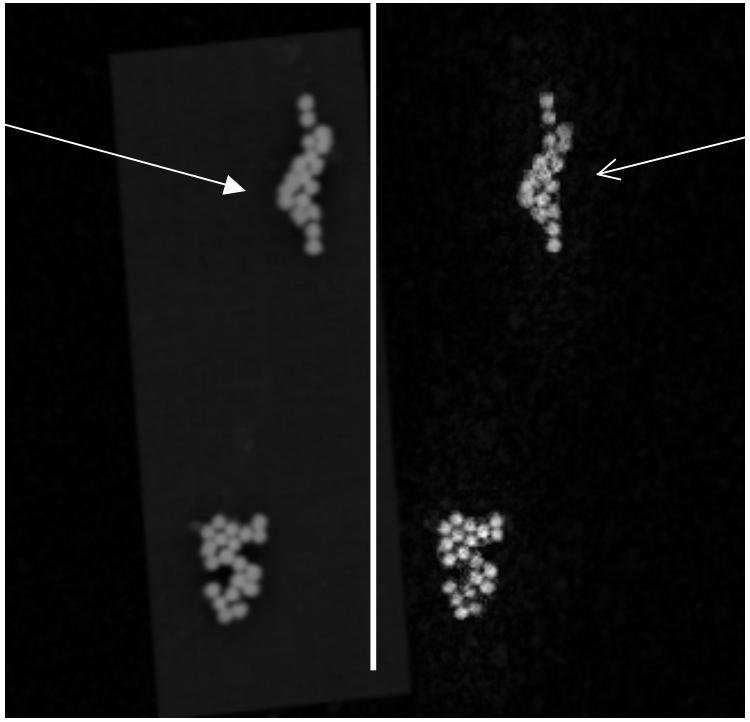

X-ray reconstruction

50 nm diameter Gold Balls on transparent SiN membrane.

No “secondary image” was used

Approximate object boundary obtained from autocorrelation fn.

*How to make an isolated object ? Use AFM to remove unwanted balls.

He, Howells, Weierrstall, Spence Chapman, Marchesini et al. Phys Rev B In press. 03, Acta A.59, 143 (2003).

Imaging of Individual Nanoparticles at the APS

Ross Harder, University of Illinois, Champaign

Coherent diffraction pattern from 170 nm Ag particle

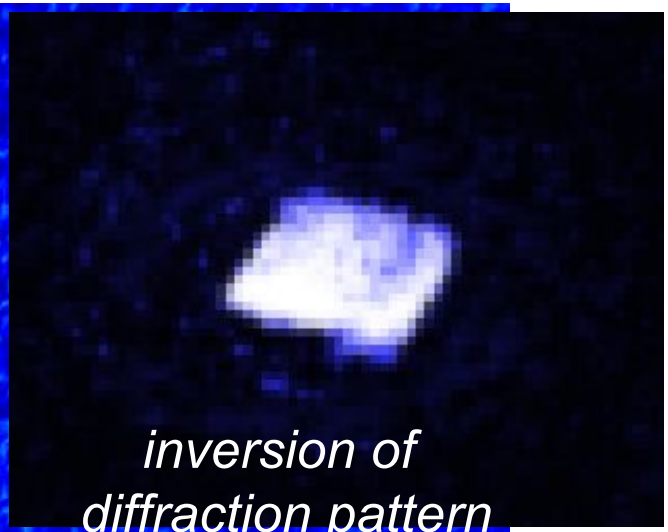

inversion of diffraction pattern 'lensless imaging'

170 nm silver cubes

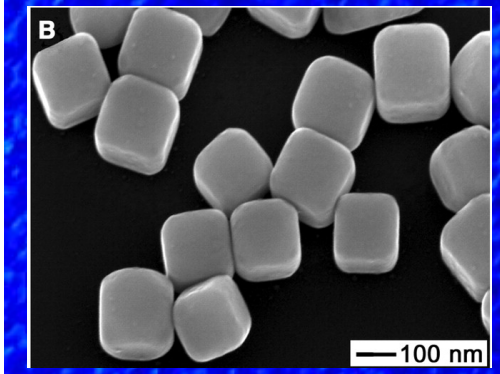

5 x 10^{-2} nm^{-1}

I.K. Robinson, et al., Science 298 2177 (2003)

Single molecule imaging?

- Atomic resolution structures known for *few* mammalian membrane proteins!
- Collect many single molecule diffraction patterns from fast x-ray pulses, and reconstruct?
- Lysozyme explodes in ~50 fsec
- R. Neutze *et al*., *Nature* **406**, 752 (2000)

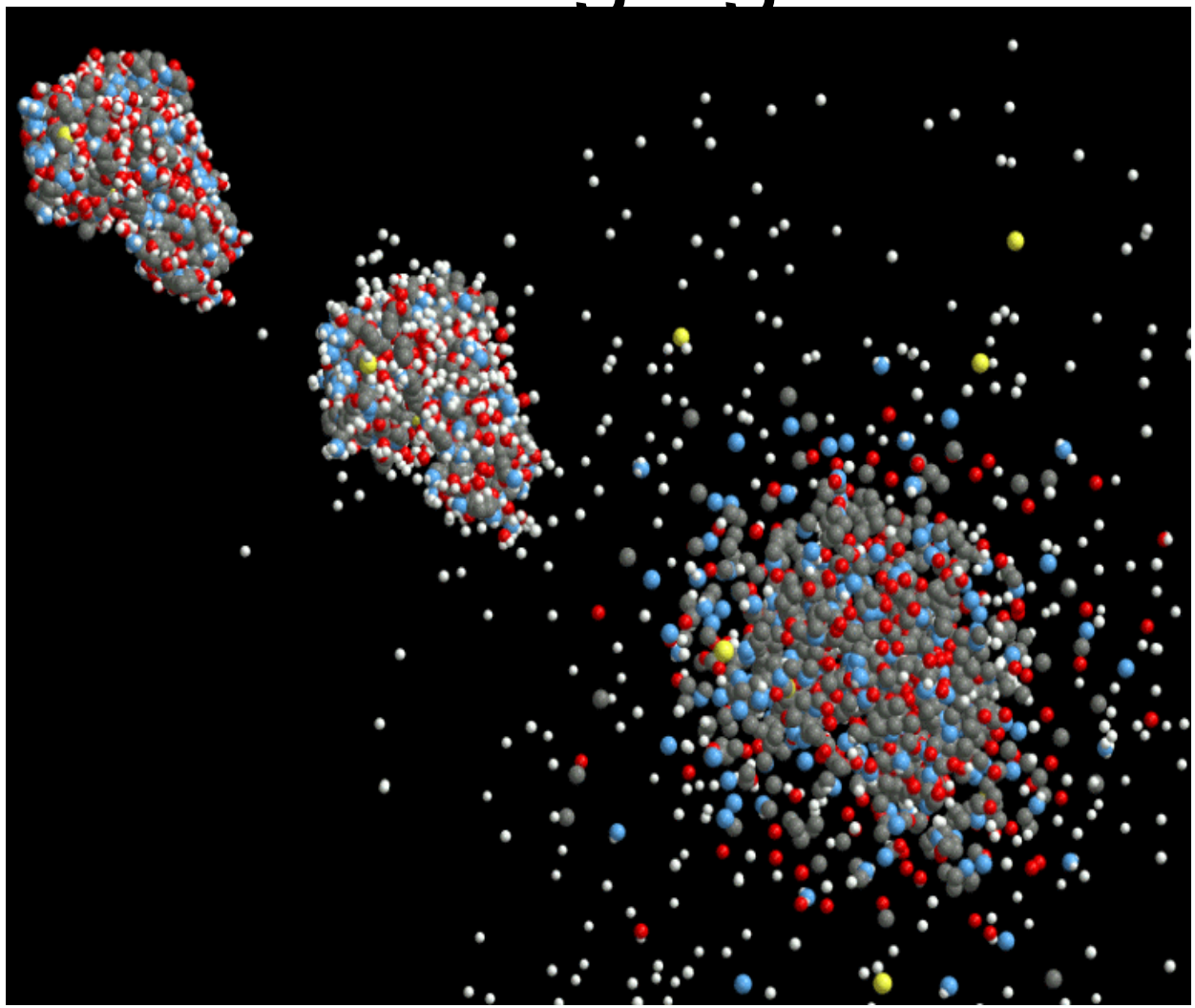

Single mimivirus particles intercepted and imaged with an X-ray laser

Beyond crystallography: A new world in structural sciences

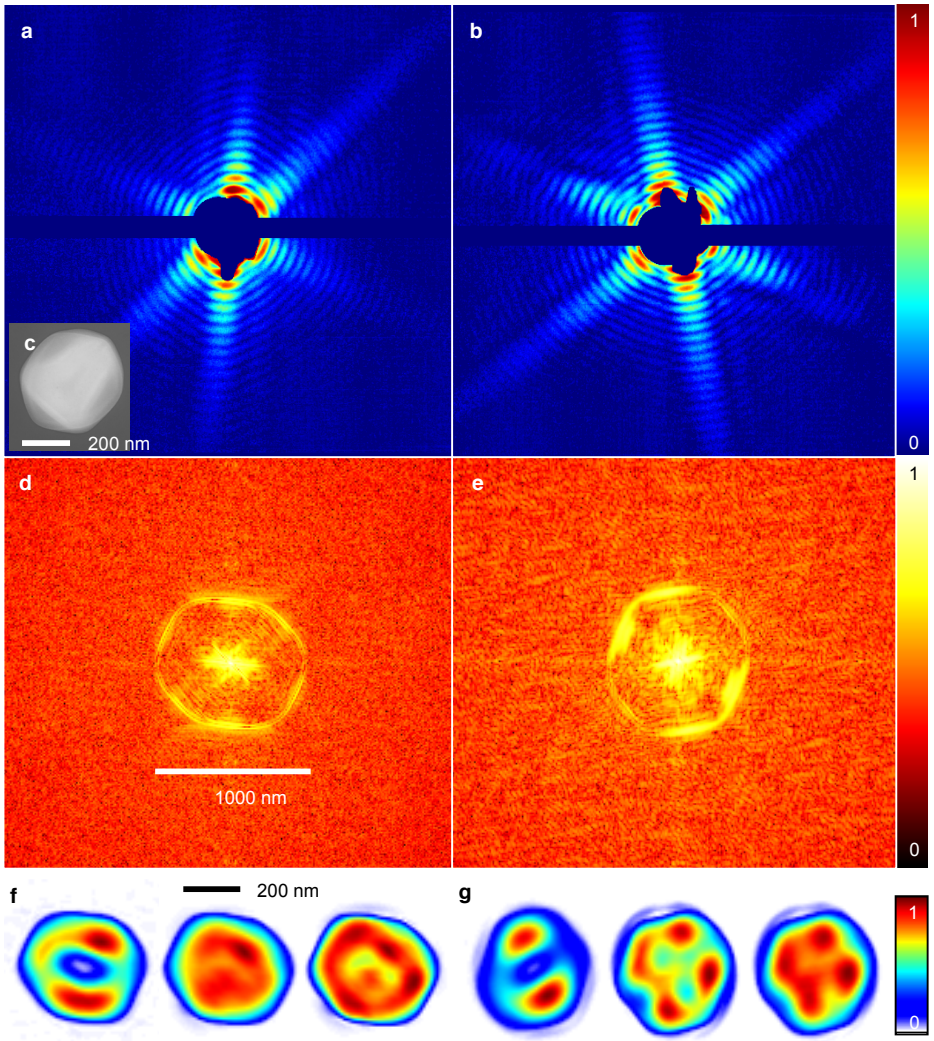

- A very short and extremely bright coherent X-ray pulse can be used to outrun key damage processes and obtain a single diffraction pattern from a large macromolecule, a virus, or a cell *without the need for crystalline periodicity.*
- Mimivirus is the largest known virus, *comparable in size to a small living cell*. It is too big for structure determination by electron microscopy and it cannot be crystallised.
- The structure of the intact virus was recovered from the flash diffraction pattern alone.
- There was no measurable sample deterioration.
- Death-rays: We expect high-resolution structures in such experiments with shorter and brighter photon pulses focused to a smaller area.
- Resolution can be further extended by averaging for samples available in multiple identical copies.

M.M. Seibert, T. Ekeberg, F.R.N.C Maia et al., *Nature* **470**, 78–81 (2011)

Femtosecond x-ray nanocrystallography overcomes limitations of radiation damage

A new paradigm opens up macromolecular structure determination to systems too small or radiation sensitive for synchrotron studies, and may save years of effort in crystallization trials

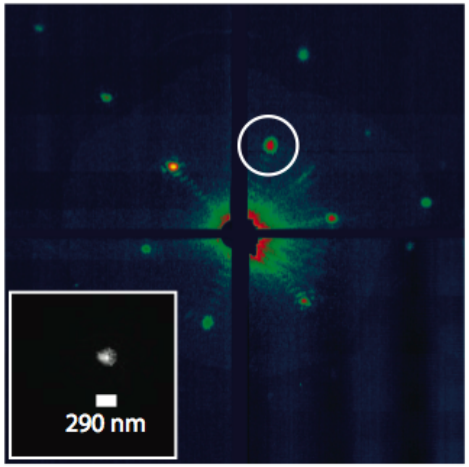

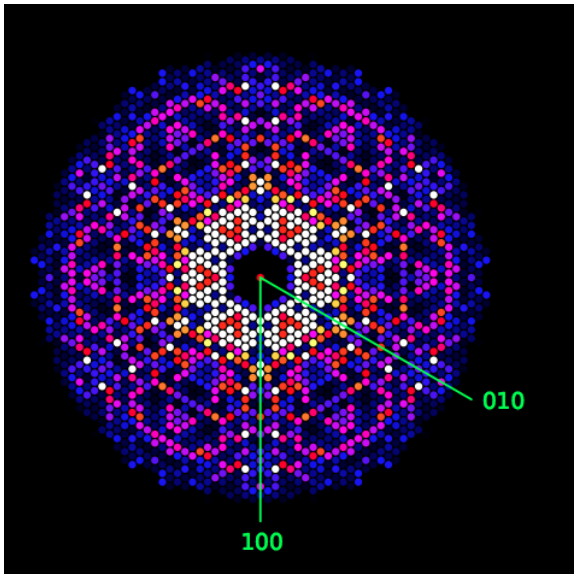

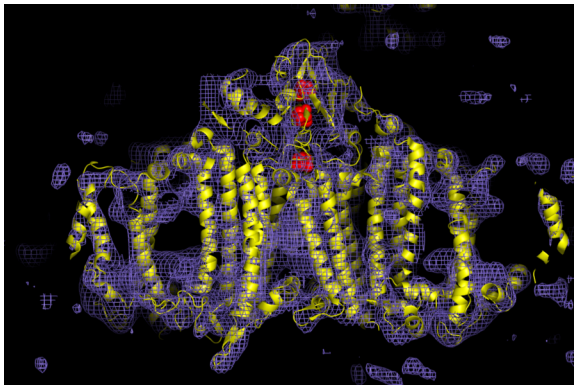

Single-shot diffraction patterns are recorded with 70 fs pulses. Coherent diffraction shows the crystal size is sub-micron (top left) and that the crystal has a perfect lattice. Individual shots are oriented in 3D and combined to build up the full information content of the underlying macromolecule (top right). This first demonstration was carried out at 2 keV photon energy, limiting the resolution to about 9 Å. (This will be improved with the dedicated CXI instrument.) The quality of the data are demonstrated by carrying out molecular replacement refinement (right). Structural details such as helices can be observed.

- The ultrafast LCLS x-ray pulses allow us to record "diffraction before destruction" where information is obtained before the onset of structural damage.
- Diffraction can be measured from sub-micron crystals containing less than a thousand molecules.
- Demonstrated using Photosystem I, a membrane protein, key to photosynthesis, that is extremely difficult to grow into large crystals.
- 30 single-crystal patterns per second were recorded from a liquid stream carrying a suspension of nanocrystals. 15,000 of these were indexed and combined into a full diffraction pattern which was analyzed with standard tools.
- Data are collected at room temperature. No cryogenic cooling or stabilization required.

Linac Coherent Light Source H.N. Chapman et al., Nature **470,** 73 (2011)

[redacted]

SLAC NATIONAL ACCELERATOR LABORATORY

LCLS Experiment 1 - Oct 1, 2009

Nature of the electronic response to

10^5 x-rays/Å^2
80 - 340 fs
800 - 2000 eV

~10^{18} W/cm^2

Original single molecule imaging parameters, Neutze et al. Nature (2000)
3 x 10^{12} x-rays/(100 nm)^2 = 3 x 10^6 x-rays/Å^2
10 fs
~10^{22} W/cm^2

Femtosecond electronic response of atoms to ultraintense x-rays

Understanding the response of matter to ultraintense x-ray irradiation is vital for LCLS applications

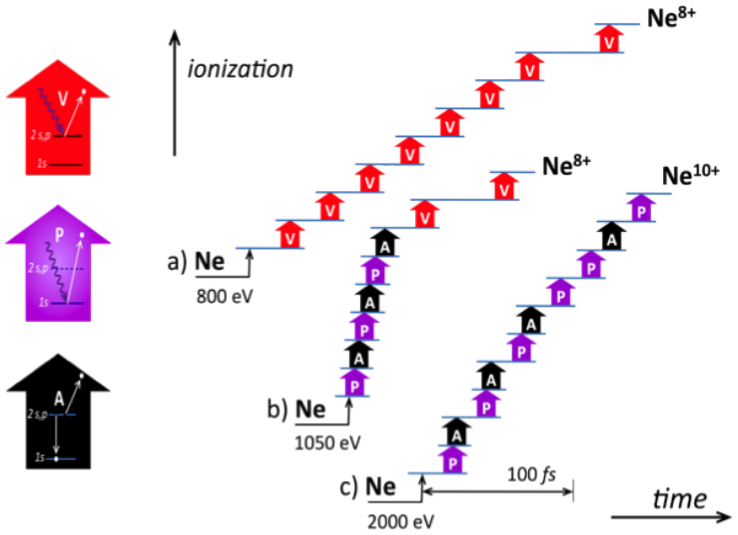

Multiphoton ionization of atoms occurs within a single LCLS pulse of ~100 fs duration and fluence of ~10^{12} x-rays per square micron. The multiple ionization proceeds through a sequence of single electron ejections. Three types of electrons are ejected, valence (V), inner-shell (P) and Auger (A),as depicted on the left of the diagram. One can control the ionization mechanism. Studying the prototypical neon atom: at photon energies below the K-edge (870 eV) the outer electrons are stripped (VVV… process), whereas at photon energies above the K-edge the inner electrons are initially ejected, followed by femtosecond Auger decay (PAPA… process). At very high intensity, both 1s core electrons can be removed prior to refilling by Auger decay to produce exotic hollow atoms.

- LCLS provides x-ray pulses with peak intensities more than a billion times greater than those from any existing synchrotron source. Understanding the electronic response at extreme x-ray intensities is fundamental.
- By studying a simple target, neon, where the dominant interaction changes as a function of photon energy from outer- to inner-shell absorption, a general understanding can be achieved.
- Observe full stripping of neon via a six-photon, ten-electron process within a single ~100 fs x-ray pulse – the first observed multiphoton x-ray process.
- Observe x-ray induced transparency via hollow atom formation at high x-ray intensities – predict this phenomenon will be generally observed in molecules, solids – allowing one to control the penetration depth in matter with pulse duration.
- Straightforward rate equation model reproduces the observed trends – suggesting that more complex systems may be modeled.

L. Young et al., Nature **466,** 56 (2010)

[redacted]

SLAC NATIONAL ACCELERATOR LABORATORY

Hollow atom production: deliberate, huge and an a an indicator of x-ray pulse duration

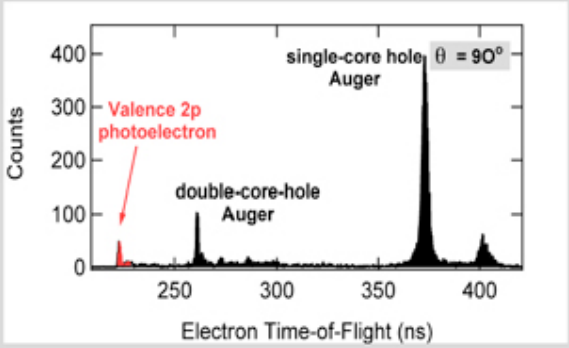

Hollow atom yield
@ LCLS ~10%
@ synchrotron ~0.3%
due to electron correlation

1050 eV,
nominal electron bunch
duration ~80 fs

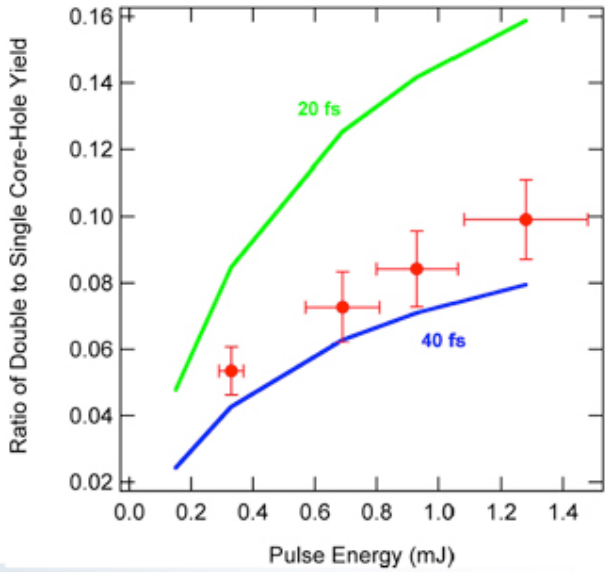

Summary of ultra-intense x-ray interaction phenomena

- Target changes during a single 100 fs x-ray pulse at fluences similar to that for single molecule imaging
  - six-photon, ten-electron stripping of neon (~$10^{12}/\mu m^2$)
  - multiphoton absorption probability high when fluence > $1/\sigma$
- Intensity-induced x-ray transparency – a general phenomena
  - transient x-ray transparency caused by formation of hollow atoms
  - hollow atoms $\sigma_{scatt}/\sigma_{abs}$ is increased – advantageous for imaging
- Straightforward rate equation calculations capture essential physics
- Femtosecond time-scale atomic processes provide FEL diagnostics

First realization of an atomic inner-shell x-ray laser at 850 eV, by ultrafast photoionization of Neon with the LCLS

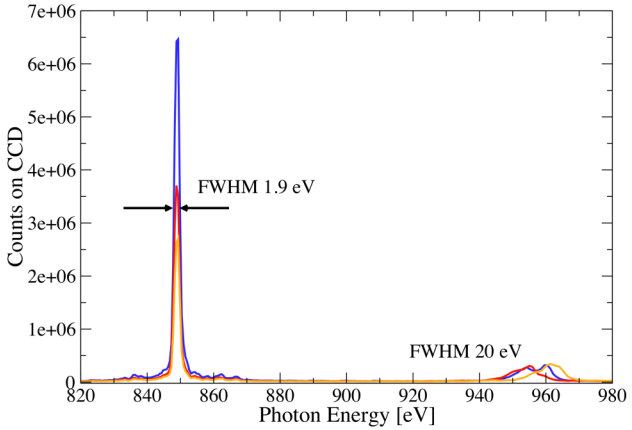

Single shot spectra of the transmitted LCLS line at around 960 eV and the Ne K-a line at 850 eV (1.9 eV instrument-limited width). The brightest shot resulted in 2x10^{9} photons in the Ne K-a line, with a conversion efficiency of 10^{-3}.

- The photoionization-based atomic x-ray lasing scheme was first proposed in 1967 (Duguay and Renzepis)
- Due to requirement of an extremely fast and intense x-ray pump source, it could never be realized so far.
- The experiment is a first step in the virtually unexplored field of non-linear quantum optics with x-rays and opens the pathway to new, non-linear spectroscopic methods in the x-ray regime

- Focusing LCLS pulses of 960 eV into a Neon gas sample to a spot size of ~1.5 mm, a long narrow plasma column is produced on a femtosecond timescale by photoionization of the K-shell, resulting in a population inversion of the Ne K-a transition.
- Fluorescence photons of the front-end of the plasma column get amplified by stimulated emission, resulting in ultrabright, fs x-ray pulses at 850 eV

Peak intensity of the Ne K-a line as a function of the pumping power of the LCLS. Doubling the pumping intensity gives a rise in the peak power of four orders of magnitude.

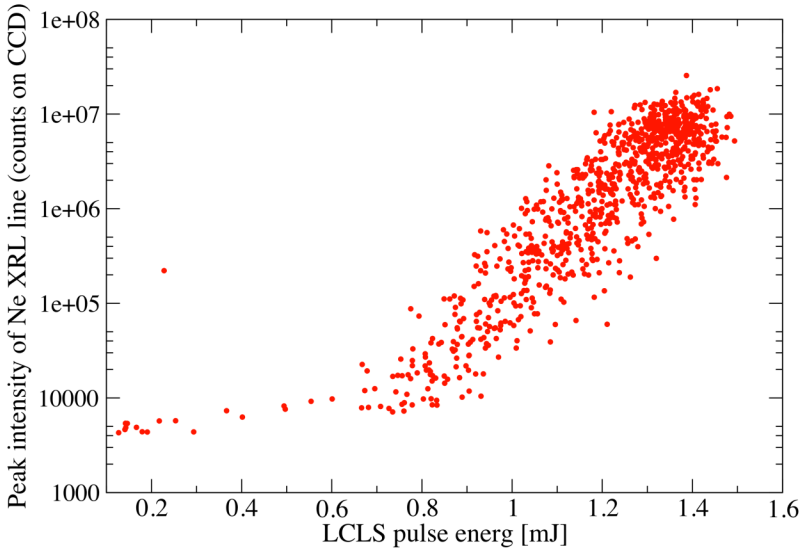

N. Rohringer et al., manuscript in preparation

Controlling magnetism in complex oxide with lattice excitation

New approach for magnetic switching disclosed at the LCLS Free Electron Laser

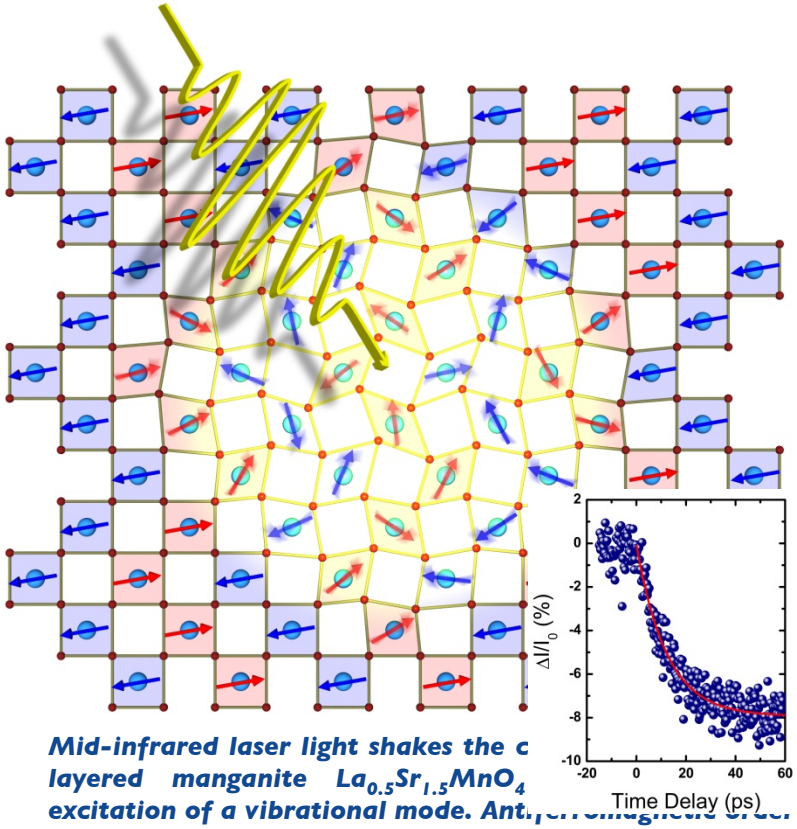

Mid-infrared laser light shakes the c layered manganite $La_{0.5}Sr_{1.5}MnO_4$ excitation of a vibrational mode. Anti[illegible] is in this way perturbed, as viewed by time-resolved resonant soft X-ray diffraction from the magnetic superlattice.

- To date, light control of magnetization has always been induced by near-infrared light. This type of stimulation is associated with large dissipation, as eV-photon energies are used to drive the rearrangement of the microscopic order on the meV energy scale.
- Electronic properties of complex oxides can be controlled by optical excitation of lattice vibrations in the mid infrared, providing an alternate path to steer condensed matter on ultrafast timescales.
- Recent experiments at the LCLS Free Electron Laser utilizing time-resolved resonant soft X-ray diffraction demonstrate that the magnetic order in complex oxides can be disordered through optical lattice manipulation.
- The magnetic response time is 12ps, likely dictated by spin-lattice relaxation rates.

LCLS | CFEL SCIENCE | Center for Free-Electron Laser Science | BROOKHAVEN NATIONAL LABORATORY | BERKELEY LAB | ALS

Linac Coherent Light Source

M. Först, R.I. Tobey, S. Wall et al., to be published

SLAC NATIONAL ACCELERATOR LABORATORY

LCLS pump-probe experiments: CO on Ru(001)

- Nearly all chemical reactions of importance to society occur at interfaces
- Catalysis is a trillion dollar industry and is also at the core of chemical energy transformations
- The first pump probe experiment at LCLS investigated a simple reaction step involving breaking of the CO-metal bond
- The experiments use a 400 nm optical laser pump pulse, and a LCLS pulses to probe the CO electronic structure state though O K-emission spectroscopy as a function of time delay.
- The results shows the time evolution of a transient CO state where the chemical bond strength to the surface is reduced

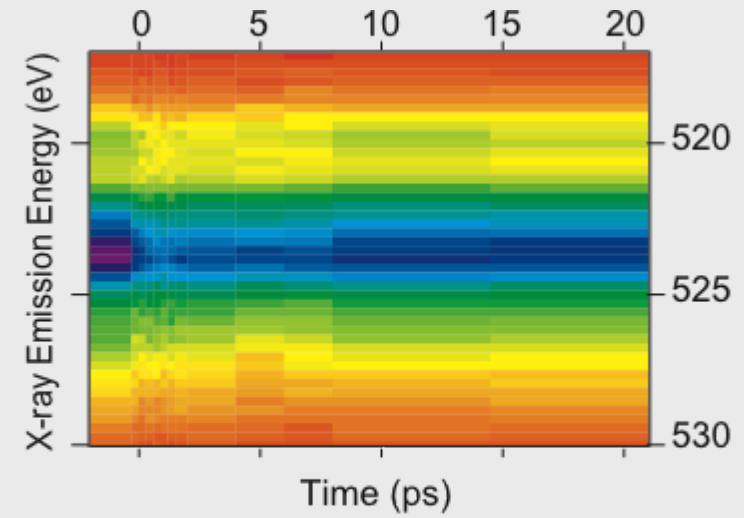

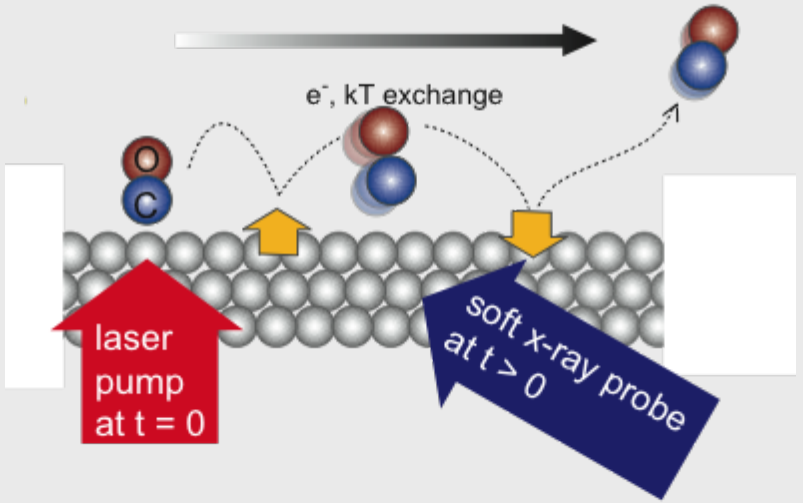

PIs: Anders Nilsson, Hirohito Ogasawara, Dennis Nordlund (SLAC), Wilfried Wurth (DESY), Alexander Föhlish (Helmholtz center), Henrik Öström (Sockholm U) and Martin Wolf (Fritz Haber Institute)

Conclusion

Much of the most exciting recent science with Neutrons and X-rays has resulted from fruitful collaborations between accelerator physicists and CM and Materials Scientists and Crystallographers and Biologists

Hopefully, this will continue, leading to more exciting science over the next decade,
So, this is not……..

THE END